NACA RM L52B25

NACA

RESEARCH MEMORANDUM

EFFECTS OF HORIZONTAL-TAIL POSITION AND ASPECT RATIO ON LOW-SPEED STATIC LONGITUDINAL STABILITY AND CONTROL CHARACTERISTICS OF A 60° TRIANGULAR-WING MODEL HAVING TWIN TRIANGULAR ALL-MOVABLE TAILS

By Byron M. Jaquet

Langley Aeronautical Laboratory
Langley Field, Va.

NATIONAL ADVISORY COMMITTEE
FOR AERONAUTICS
WASHINGTON

May 23, 1952
Declassified October 12, 1954.

NATIONAL ADVISORY COMMITTEE FOR AERONAUTICS

RESEARCH MEMORANDUM

EFFECTS OF HORIZONTAL-TAIL POSITION AND ASPECT RATIO ON LOW-SPEED STATIC LONGITUDINAL STABILITY AND CONTROL CHARACTERISTICS OF A 60° TRIANGULAR-WING MODEL HAVING TWIN TRIANGULAR ALL-MOVABLE TAILS

By Byron M. Jaquet

SUMMARY

A low-speed investigation has been made in the Langley stability tunnel to determine the effects of tail height, length, and aspect ratio on the static longitudinal stability and control characteristics of a 60° triangular-wing model having twin triangular all-movable tails located near the wing tips.

A tail position below the wing-chord plane had more favorable static longitudinal stability than either of the two positions above the wing-chord plane. A tail position high above the wing-chord plane generally had satisfactory static longitudinal stability up to high lift coefficients; whereas twin tails located in an intermediate position were adversely affected by the wing vortex flow and, consequently, large decreases in stability occurred for this tail position.

With the center of gravity at a common location (quarter chord of the mean aerodynamic chord) for all model configurations a reduction in tail aspect ratio from 2.31 to 1.07 produced a decrease in stability at low lift coefficients as would be expected. On the basis of equal stability at zero lift (a different center of gravity for each model configuration), however, a decrease in aspect ratio caused an increase in stability at moderate and high lift coefficients. This behavior is believed to be associated with the different spanwise extents of the horizontal tails and a resultant difference in average downwash and dynamic pressure at the tail.

A tail position below the wing-chord plane was the most favorable with respect to pitching-moment effectiveness inasmuch as maximum effectiveness, which was essentially constant with lift coefficient,

was attained in this position. A reduction in tail aspect ratio generally resulted in a decrease in pitching-moment effectiveness through the lift-coefficient range.

For a tail position below the wing-chord plane twin tails of aspect ratio 2.31 produced higher trim lift coefficients than twin tails of aspect ratio 1.07. In tail positions above the wing-chord plane, however, the aspect-ratio-1.07 tails produced the highest trim lift coefficients. The aspect-ratio-2.31 tails produced slightly higher trim-lift-curve slopes at zero angle of attack than the aspect-ratio-1.07 tails.

Twin tails of aspect ratio 2.31 had less change in static longitudinal stability with lift coefficient than a single tail of aspect ratio 2.31. At low and moderate lift coefficients, the twin tails had about the same pitching-moment effectiveness as the single tail of the same aspect ratio; whereas at high lift coefficients the single tail had greater pitching-moment effectiveness.

INTRODUCTION

Low-scale and full-scale investigations have indicated that triangular-wing airplanes equipped with twin vertical fins have the most satisfactory static longitudinal stability when the fins are located as close to the wing tips as possible (see references 1 and 2). The longitudinal control characteristics of triangular-wing configurations equipped with twin vertical fins have not been determined although the investigation of reference 3 has indicated adverse effects of the vortex flow on the control effectiveness and hinge-moment characteristics of constant-chord controls; the control effectiveness and hinge moments varied erratically with angle of attack. Possibly a control separated from the wing would be relatively unaffected by the vortex flow.

In a low-speed investigation (reference 4) of a 60° triangular-wing model having various triangular-horizontal-all-movable tails located behind the center of gravity, the optimum positions from a standpoint of static longitudinal stability were high and forward and low and rearward. The former position was one of relatively low control effectiveness and the latter, although having good control effectiveness, would severely restrict the landing angle. Twin all-movable controls located above or slightly below the wing tips would not seriously restrict the landing angle and would also be available for use as ailerons.

The present investigation was conducted, therefore, to determine the advantages or disadvantages of twin all-movable tails from the standpoint of static longitudinal stability and pitching-moment effectiveness. Included in the investigation was the determination of the effects

of tail height, tail length, and tail aspect ratio for a 60° triangular-wing model equipped with twin all-movable tails of triangular plan form. The results for the twin tails were compared with the results for a single tail (reference 4) of the same area and aspect ratio in the same tail position.

SYMBOLS

The data presented herein are in the form of standard NACA symbols and coefficients of forces and moments and are referred to the stability system of axes with the origin at the projection of the quarter-chord of the mean aerodynamic chord on the plane of symmetry unless otherwise specified. The positive direction of the forces, moments, and angular displacements is indicated in figure 1. The coefficients and symbols used herein are defined as follows:

C_L	lift coefficient (L/qS)
C_{L_t}	trim lift coefficient
C_m	pitching-moment coefficient $(M/qS\bar{c})$
L	lift, pounds
M	pitching moment, foot-pounds
A	aspect ratio (b^2/S)
b	span, feet
S	wing area, square feet
S_H	area of one horizontal tail, square feet
c	local chord parallel to plane of symmetry, feet
$\bar{c}$	mean aerodynamic chord, feet $\left(\frac{2}{S}\int_0^{b/2} c^2 dy\right)$
c_r	root chord, feet
q	free-stream dynamic pressure, pounds per square foot $\left(\frac{\rho V^2}{2}\right)$

V	free-stream velocity, feet per second
ρ	density of air, slugs per cubic foot
y	spanwise distance measured from, and perpendicular to, plane of symmetry, feet
l	tail length (distance between quarter-chord point of wing mean aerodynamic chord and quarter-chord point of tail mean aerodynamic chord measured parallel to fuselage center line), feet
z	tail height (height of tail above or below wing-chord plane), feet
α	angle of attack of wing-chord plane, degrees
α_t	trim angle of attack, degrees
i_t	symmetrical deflection of left and right tails with respect to wing-chord plane, degrees
Λ_{LE}	angle of sweepback of leading edge, degrees
$C_{L_\alpha} = \frac{\partial C_L}{\partial \alpha}$	
$C_{L_{\alpha_t}}$	trim-lift-curve slope
$C_{L_{i_t}} = \frac{\partial C_L}{\partial i_t}$	
$C_{m_{C_L}} = \frac{\partial C_m}{\partial C_L}$	
$C_{m_{i_t}} = \frac{\partial C_m}{\partial i_t}$	
H_1	horizontal tail 1 (see fig. 2)
H_2	horizontal tail 2 (see fig. 2)

APPARATUS, MODEL, AND TESTS

The present investigation was conducted in the 6- by 6-foot test section of the Langley stability tunnel. The model was mounted on a single-strut support with the pivot point at the quarter chord of the mean aerodynamic chord. The strut was attached to a six-component balance system.

The model consisted of a mahogany wing-fuselage combination and two separate arrangements of twin horizontal tails. The wing had an aspect ratio of 2.31, $\Lambda_{LE} = 60^{\circ}$, and modified NACA $65_{(06)}$-006.5 airfoil sections parallel to the plane of symmetry. The fuselage had a circular cross section and a fineness ratio of 7.38. Additional details of the fuselage may be obtained from reference 2. One pair of tails consisted of two tails of aspect ratio 2.31, $\Lambda_{LE} = 60^{\circ}$, and $\frac{S_H}{S} = 0.05$ designated as $2H_1$ and the other pair consisted of two tails of aspect ratio 1.07, $\Lambda_{LE} = 75^{\circ}$, and $\frac{S_H}{S} = 0.05$ designated as $2H_2$. Each pair of tails was investigated at three tail heights for each of two tail lengths. The tails were supported by $\frac{1}{4}$- by 2-inch steel support struts (one strut was used for each height) mounted on 1- by $2\frac{3}{16}$- by 16-inch mahogany booms with the center line of the booms at $0.74\frac{b}{2}$ from the plane of symmetry. (This spanwise position was selected because vertical fins so placed were least affected by vortex flow (references 1 and 2).) Pertinent details of the model, horizontal tails, and tail positions are shown in figure 2. Photographs of several model configurations are presented in figure 2.

The force tests consisted of measurement of lift and pitching moment through an angle-of-attack range of -4° to 36° for several angles of incidence of the horizontal tails. All force tests were made at a dynamic pressure of 39.7 pounds per square foot, a Mach number of 0.17, and a Reynolds number of 2.06×10^6.

Tuft-grid photographs (see reference 5 for details of the tuft-grid procedure) for several model configurations were made with an aerial camera mounted in the tunnel about 50 feet downstream from the model. These tests were made at a dynamic pressure of 8 pounds per square foot and a Reynolds number of 0.92×10^6. A photograph of the tuft grid mounted in the tunnel is presented in figure 3.

CORRECTIONS

Approximate jet-boundary corrections based on unswept-wing concepts have been applied to the angle of attack. Complete-model (tail on) pitching moments have been corrected for the effects of the jet boundaries by the methods of reference 6 and the dynamic pressure was corrected for blockage effects by the methods of reference 7. The data have not been corrected for the effects of the support strut.

RESULTS AND DISCUSSION

Preliminary Remarks

The lift and pitching-moment data, with respect to $\bar{c}/4$, for the various model configurations are presented in figures 4 to 15 for several angles of incidence of the horizontal tails. For convenience, the pitching-moment coefficients at $i_t = 0^{\circ}$ of figures 4 to 15 are replotted in figures 16 and 17. To enable the determination of the effects of tail height, length, and aspect ratio on the basis of equal stability at $C_L = 0$ the data of figures 16 and 17 have been recomputed about a different center-of-gravity position for each configuration to give $C_{m_{C_L}} = -0.10$ at $C_L = 0$ and these data are presented in figures 18 and 19. The centers of gravity for each model configuration having $2H_1$ in figure 18 are as follows:

$l/\bar{c}$	$z/\bar{c}$	Center of gravity (percent $\bar{c}$)
0.75	-0.16	32.5
	.16	31.8
	.40	32.1
1.00	-0.16	34.6
	.16	33.8
	.40	34.0

The centers of gravity for configurations having $2H_2$, data for which are presented in figure 19, are as follows:

$l/\bar{c}$	$z/\bar{c}$	Center of gravity (percent $\bar{c}$)
0.75	-0.16 .16 .40	31.5 30.1 31.5
1.00	-0.16 .16 .40	32.0 31.5 32.0

The wing-fuselage center of gravity is at $0.275\bar{c}$ for $C_{m_{C_L}} = -0.10$.

Longitudinal Stability

Effect of tail height and length.- From figures 16 and 17, it can be seen that the wing-fuselage combination is longitudinally stable through the lift-coefficient range. At low and moderate lift coefficients, the static stability of the model configuration having twin tails $(2H_1$ or $2H_2)$ was relatively unaffected by a change in tail height except for $\frac{z}{\bar{c}} = 0.16$ where the tail surfaces entered the wake region of the wing at moderate lift coefficients and a noticeable decrease occurred in stability. This decrease in stability was more pronounced for the shorter tail length.

The data of figures 18 and 19 $\left(C_{m_{C_L}} = -0.10 \text{ at } C_L = 0\right)$ indicate that the low tail position $\left(\frac{z}{\bar{c}} = -0.16\right)$ and the very high position $\left(\frac{z}{\bar{c}} = 0.40\right)$ provide about the same variation in stability with lift coefficient for a tail length of $\frac{l}{\bar{c}} = 0.75$. For a tail length of $\frac{l}{\bar{c}} = 1.00$ the low tail position and very high position have about the same variation of stability with lift coefficient up to lift coefficients near maximum where a decrease occurs for the high position. For both tail lengths a decrease in stability occurs at moderate lift coefficients for the intermediate tail position $\left(\frac{z}{\bar{c}} = 0.16\right)$.

The effect of tail location on the change in longitudinal stability between $C_L = 0$ and $C_L = 0.8$ is summarized in figure 20. Also included in figure 20 are data for the single all-movable tail of aspect ratio 2.31 which were obtained from reference 4. The most favorable positions for the tails are either $\frac{z}{\bar{c}} = -0.16$ where there is no change in stability for $2H_1$ and stabilizing changes for $2H_2$ or $\frac{z}{\bar{c}} = 0.40$ where, although destabilizing, the changes in the aerodynamic center for either $2H_1$ or $2H_2$ are less than 2 percent of the mean aerodynamic chord. The greatest change in stability occurs for $\frac{z}{\bar{c}} = 0.16$ for both $2H_1$ and $2H_2$. For the range of high tail positions for which comparison of the twin and single tails is possible, it appears that the twin tails have less change in stability between $C_L = 0$ and $C_L = 0.8$.

The changes in stability which occur, for tail-on configurations, at moderate and high lift coefficients are believed to be a result of large increases of the rate of change of downwash angle with angle of attack which occurred for the single tails reported in reference 4. Wake measurements in the vicinity of the horizontal tails indicated erratic variations in downwash angle and dynamic pressure at the tail because of the proximity of the trailing vortex system and thus these data are not presented. Some indication of the effects of downwash on stability can be determined from the tuft-grid photographs presented as figure 21. These photographs were made at a Reynolds number of 0.92×10^6; whereas the force tests were made at a Reynolds number of 2.06×10^6. Tuft-grid photographs are presented only for $\frac{l}{\bar{c}} = 0.75$ and the configurations having $2H_1$ inasmuch as no appreciable difference in the flow patterns was discernible. The grid was located 1 foot behind the wing trailing edge. The tufts are 3 inches long and spaced at 1-inch intervals vertically and horizontally.

From figure 21, the familiar vortex associated with triangular wings is seen to appear at the tips of the wing at $\alpha = 4^\circ$ and to increase in size and move toward the plane of symmetry as the angle of attack is increased. Vortices are also visible at the tips of the tails although they do not appear until about $\alpha = 8^\circ$ for $i_t = 0^\circ$. The delay in the formation of the vortices is probably due to the larger leading-edge radius of the tails as compared with the wing leading-edge radius. For $\frac{z}{\bar{c}} = -0.16$ and $i_t = 0^\circ$, the tails are relatively unaffected by the wing vortices at angles of attack up to about 20°. At higher angles of attack, it appears that the tails are in regions of upwash over the inboard semispan and downwash over the outboard semispan. When the tails are

deflected -20°, vortices are visible on each tip of the tails at $\alpha = 0^{\circ}$. As the angle of attack is increased, the vortices on the outboard tip of the tails are displaced upward and both inboard and outboard tip vortices decrease in size. At high angles of attack, the tails are in regions of upwash and, thus, are more effective; thereby an increase in stability results. For a tail height of $\frac{z}{\bar{c}} = 0.16$, the tails are almost completely engulfed by the wing vortices even at an angle of attack as low as 8°. The large changes in downwash angle with angle of attack result in large decreases in stability. When the tails are located high above the wing-chord plane $\left(\frac{z}{\bar{c}} = 0.40\right)$, they do not become completely engulfed by the wing vortices until an angle of attack of 36° is reached. Thus, this tail position affords relatively good longitudinal stability characteristics (figs. 18 and 19).

Effect of tail aspect ratio.- With the center of gravity of each configuration at the same location $(\bar{c}/4)$ a reduction in tail aspect ratio from 2.31 $(2H_1)$ to 1.07 $(2H_2)$ produced a decrease in stability at low lift coefficients as would be expected (figs. 16 and 17). On the basis of equal stability at $C_L = 0$ (a different center-of-gravity position for each configuration), however, a decrease in aspect ratio caused an increase in stability at moderate and high lift coefficients (figs. 18 and 19). This behavior is believed to be associated with the different spanwise extents of the horizontal tails and a resultant difference in average downwash and dynamic pressure at the tail. For the intermediate tail height $\left(\frac{z}{\bar{c}} = 0.16\right)$ of the higher-aspect-ratio tails (2.31), the decrease in stability at moderate lift coefficients was much more severe than the decrease in stability that occurred for the low-aspect-ratio tails. (Compare figs. 16 and 17, and 18 and 19.)

Longitudinal Control Effectiveness

Effect of tail height and length.- The control parameters $C_{L_{i_t}}$ and $C_{m_{i_t}}$ were measured through $i_t = 0^{\circ}$. The slopes were generally linear between $i_t = 10^{\circ}$ and -20°, however. The control-effectiveness data for each model configuration were recomputed about different center-of-gravity positions to give $C_{m_{C_L}} = -0.10$ at $C_L = 0$ and, thus, the data are directly indicative of the effects of tail height and length on the control effectiveness. (See the section entitled "Preliminary Remarks" for the center-of-gravity positions.)

The change in lift with tail incidence $C_{L_{i_t}}$ and the pitching-moment effectiveness $C_{m_{i_t}}$ varied considerably with lift coefficient depending on the tail position (fig. 22). In the investigation reported in reference 4 it was found that these parameters were relatively constant up to maximum lift for a single all-movable tail of the same area and aspect ratio as $2H_1$ for tail heights of $\frac{z}{\bar{c}} = 0.25$ to $\frac{z}{\bar{c}} = 0.75$. At low lift coefficients, changes in tail height for the twin tails did not appreciably affect the values of $C_{L_{i_t}}$ or $C_{m_{i_t}}$. An increase in tail length from $\frac{l}{\bar{c}} = 0.75$ to $\frac{l}{\bar{c}} = 1.00$ increased $C_{m_{i_t}}$ slightly but had essentially no effect on $C_{L_{i_t}}$. For either tail length (fig. 22), a tail position below the wing-chord plane produced the largest values of $C_{L_{i_t}}$ throughout the lift-coefficient range. The value of $C_{m_{i_t}}$ decreased slightly with an increase in lift coefficient for $\frac{l}{\bar{c}} = 0.75$ and $\frac{z}{\bar{c}} = -0.16$ but did not vary appreciably with lift coefficient for the same tail height and $\frac{l}{\bar{c}} = 1.00$. An increase in tail height $\left(\text{to } \frac{z}{\bar{c}} = 0.16\right)$ for either tail length resulted in a decrease in both $C_{L_{i_t}}$ and $C_{m_{i_t}}$ in the moderate and high lift-coefficient range. For a tail length of $\frac{l}{\bar{c}} = 0.75$, the pitching-moment effectiveness was zero from about $C_L = 0.7$ past maximum lift. A further increase in tail height $\left(\text{to } \frac{z}{\bar{c}} = 0.40\right)$ generally caused an increase in $C_{L_{i_t}}$ and $C_{m_{i_t}}$ for the same range of lift coefficient.

The best pitching-moment effectiveness was obtained for a tail position of $\frac{z}{\bar{c}} = -0.16$ and $\frac{l}{\bar{c}} = 1.00$ which was also the best position from the standpoint of static longitudinal stability.

Effect of tail aspect ratio.- A comparison of figures 22 and 23 indicates that reducing the aspect ratio of the tails from 2.31 $(2H_1)$ to 1.07 $(2H_2)$ caused a decrease, through the lift-coefficient range, in the values of $C_{L_{i_t}}$ and $C_{m_{i_t}}$ for all tail positions as would be expected. The variation of $C_{L_{i_t}}$ and $C_{m_{i_t}}$ with $z/\bar{c}$ at $C_L = 0$ is presented in figure 24.

Comparison of twin and single tails.- A comparison of the variation of $C_{L_{i_t}}$ and $C_{m_{i_t}}$ with C_L for the single tail of reference 4 with the twin tails of the present investigation is presented in figure 25 for two tail positions. The tail height for the single tail was slightly higher than that for the twin tails but the investigation of reference 4 indicated only small effects of tail height for this region. The pitching-moment effectiveness of the twin and single tails of the same aspect ratio was about the same for low and moderate lift coefficients for either tail position. At high lift coefficients, the single tail had greater pitching-moment effectiveness than the twin tails.

Trim Characteristics

Effect of tail height, length, and aspect ratio.- The trim lift coefficients and trim angles of attack corresponding to a -30° incidence of the twin tails are presented in figure 26 plotted as a function of tail height. These data were determined on the basis of $C_{m_{C_L}} = -0.10$ at $C_L = 0$.

The data of figure 26 indicate that for the twin tails of aspect ratio 2.31 at a tail length of $\frac{l}{\bar{c}} = 0.75$ an increase in tail height increased the trim lift coefficient C_{L_t}. An increase in tail length length to $\frac{l}{\bar{c}} = 1.00$ produced a large increase in trim lift coefficient for the low tail position $\left(\frac{z}{\bar{c}} = -0.16\right)$ and a small increase in C_{L_t} for each of the other two tail heights investigated. A decrease in aspect ratio from 2.31 to 1.07 caused a decrease in C_{L_t} for a low tail position $\left(\frac{z}{\bar{c}} = -0.16\right)$ and a slight increase in C_{L_t} for positions above the wing-chord plane.

The variation of trim-lift-curve slope $\left(C_{L_{\alpha_t}}\right)$ with tail height is presented in figure 27 for $\alpha_t = 0^{\circ}$ and $C_{m_{C_L}} = -0.10$. When either the tail height or the tail length was increased, or when the tail aspect ratio was increased, a very slight increase occurred in the trim lift-curve slope.

CONCLUSIONS

A low-speed investigation made in the Langley stability tunnel to determine the static longitudinal stability and control characteristics

of a 60° triangular wing model having twin-triangular-all-movable tails has indicated the following conclusions:

1. A tail position below the wing-chord plane had more favorable static longitudinal stability than either of the two positions above the wing-chord plane. A tail position high above the wing-chord plane generally had satisfactory static longitudinal stability up to high lift coefficients; whereas twin tails located in an intermediate position were affected adversely by the wing vortex flow and, consequently, large decreases in stability occurred for this tail position.

2. With the center of gravity at a common location (quarter chord of the mean aerodynamic chord) for all model configurations, a reduction in tail aspect ratio from 2.31 to 1.07 produced a decrease in stability at low lift coefficients as would be expected. On the basis of equal stability at zero lift (a different center of gravity for each configuration), however, a decrease in aspect ratio caused an increase in stability at moderate and high lift coefficients. This behavior is believed to be associated with the different spanwise extents of the horizontal tails and a resultant difference in average downwash and dynamic pressure at the tail.

3. A tail position below the wing-chord plane was the most favorable with respect to pitching-moment effectiveness inasmuch as maximum effectiveness, which was essentially constant with lift coefficient, was attained in this position. A reduction in tail aspect ratio from 2.31 to 1.07 generally resulted in a decrease in pitching-moment effectiveness through the lift-coefficient range.

4. For a tail position below the wing-chord plane twin tails of aspect ratio 2.31 produced higher trim lift coefficients than twin tails of aspect ratio 1.07. In tail positions above the wing-chord plane, however, the aspect-ratio-1.07 tails produced the highest trim lift coefficients. The aspect-ratio-2.31 tails produced slightly higher trim-lift-curve slopes at zero angle of attack than the aspect-ratio-1.07 tails.

5. Twin tails of aspect ratio 2.31 had less change in static longitudinal stability with lift coefficient than a single tail of aspect ratio 2.31. At low and moderate lift coefficients, twin tails of aspect ratio 2.31 had about the same pitching-moment effectivenss as a single tail of the same aspect ratio investigated in essentially the same tail positions; whereas at high lift coefficients, the single tail had greater effectiveness.

Langley Aeronautical Laboratory
National Advisory Committee for Aeronautics
Langley Field, Va.

REFERENCES

1. McLemore, H. Clyde: Low-Speed Investigation of the Effects of Wing Leading-Edge Modifications and Several Outboard Fin Arrangements on the Static Stability Characteristics of a Large-Scale Triangular Wing. NACA RM L51J05, 1952.

2. Jaquet, Byron M., and Brewer, Jack D.: Effects of Various Outboard and Central Fins on Low-Speed Static-Stability and Rolling Characteristics of a Triangular-Wing Model. NACA RM L9E18, 1949.

3. Hawes, John G., and May, Ralph W., Jr.: Investigation at Low Speed of the Effectiveness and Hinge Moments of a Constant-Chord Ailavator on a Large-Scale Triangular Wing with Section Modification. NACA RM L51A26, 1951.

4. Jaquet, Byron M.: Effects of Horizontal-Tail Position, Area, and Aspect Ratio on Low-Speed Static Longitudinal Stability and Control Characteristics of a 60° Triangular-Wing Model Having Various Triangular-All-Movable Horizontal Tails. NACA RM L51I06, 1951.

5. Bird, John D., and Riley, Donald R.: Some Experiments on Visualization of Flow Fields Behind Low-Aspect-Ratio Wings by Means of a Tuft Grid. NACA TN 2674, 1952.

6. Gillis, Clarence L., Polhamus, Edward C., and Gray, Joseph L., Jr.: Charts for Determining Jet-Boundary Corrections for Complete Models in 7- by 10-Foot Closed Rectangular Wind Tunnels. NACA ARR L5G31, 1945.

7. Herriot, John G.: Blockage Corrections for Three-Dimensional-Flow Closed-Throat Wind Tunnels, With Consideration of the Effect of Compressibility. NACA Rep. 995, 1950. (Supersedes NACA RM A7B28.)

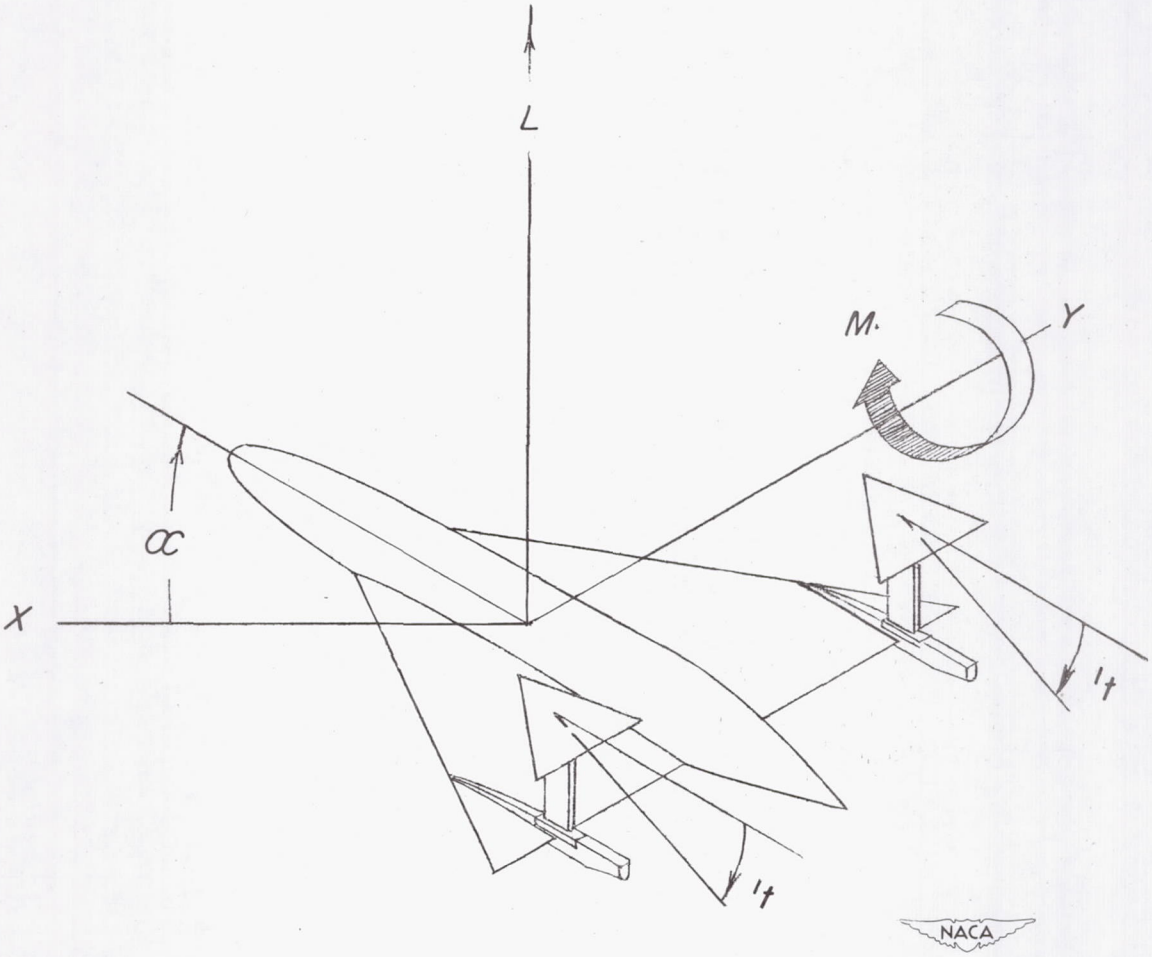

Figure 1.- Stability system of axes. Arrows indicate positive direction of forces, moments, and angular displacements.

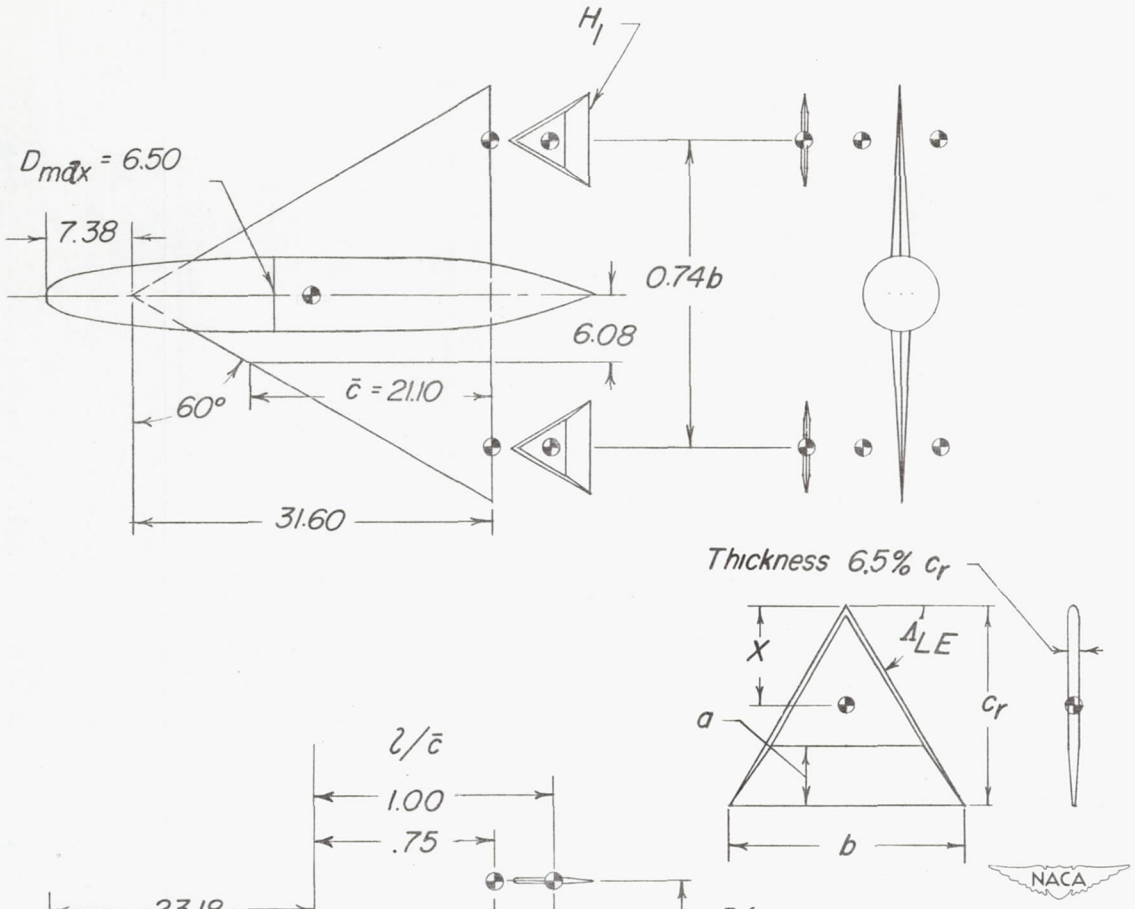

H	1	2
A	2.31	1.07
Λ_{LE} (deg)	60	75
S_H/S	.05	.05
a (in.)	2.12	3.11
b (in.)	8.16	5.56
c_r (in.)	7.06	10.38
X (in.)	3.53	5.19

(a) Pertinent details of model and horizontal tails. Aspect ratio of wing, 2.31; area of wing, 576 square inches; airfoil section of wing, NACA $65_{(06)}$-006.5; fuselage fineness ratio, 7.38. Dimensions of horizontal tails are for one only. All dimensions in inches.

Figure 2.- Geometry and photographs of models.

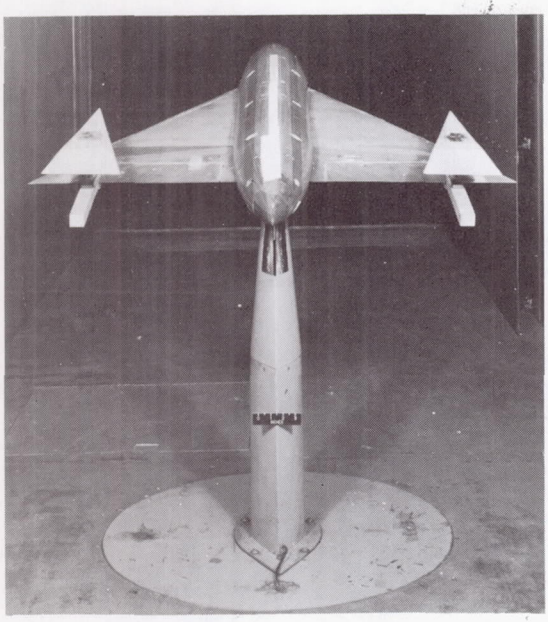

NACA
L-65559

(b) $2H_2$; $\frac{z}{\bar{c}} = 0.16$; $\frac{l}{\bar{c}} = 0.75$.

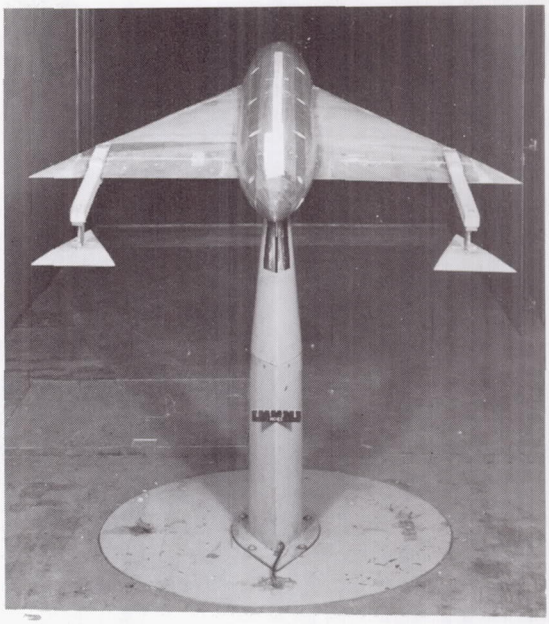

NACA
L-65560

(c) $2H_1$; $\frac{z}{\bar{c}} = -0.16$; $\frac{l}{\bar{c}} = 1.00$.

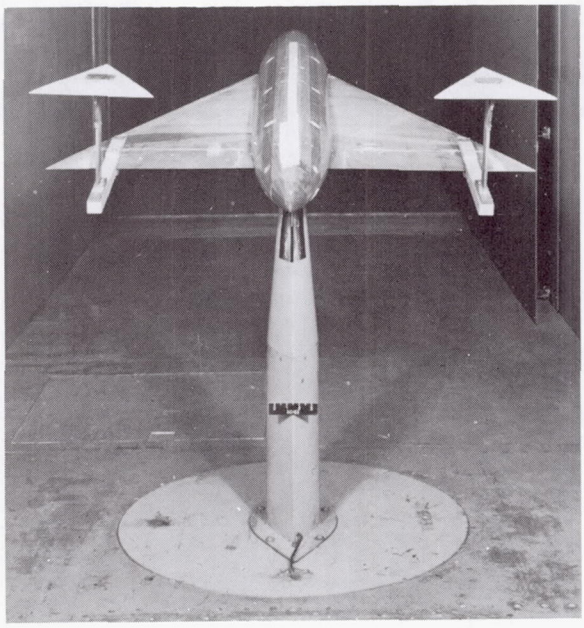

(d) $2H_1$; $\frac{z}{\bar{c}} = 0.40$; $\frac{l}{\bar{c}} = 1.00$.

NACA
L-65561

Figure 2.- Concluded.

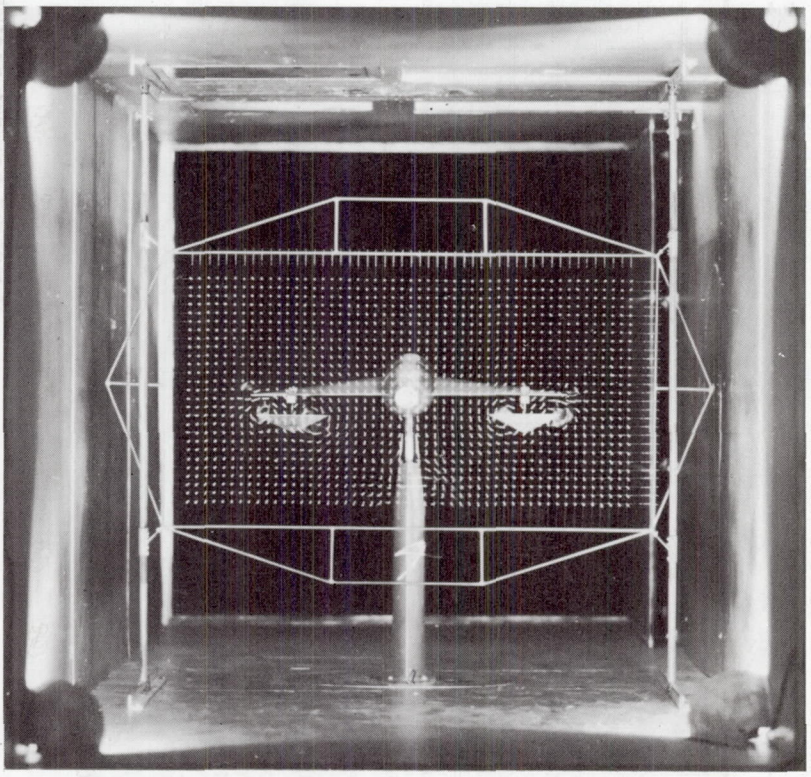

L-72745

Figure 3.- Photograph of tuft grid as mounted in 6- by 6-foot test section of Langley stability tunnel. Tufts 3 inches long and spaced 1 inch apart both vertically and horizontally.

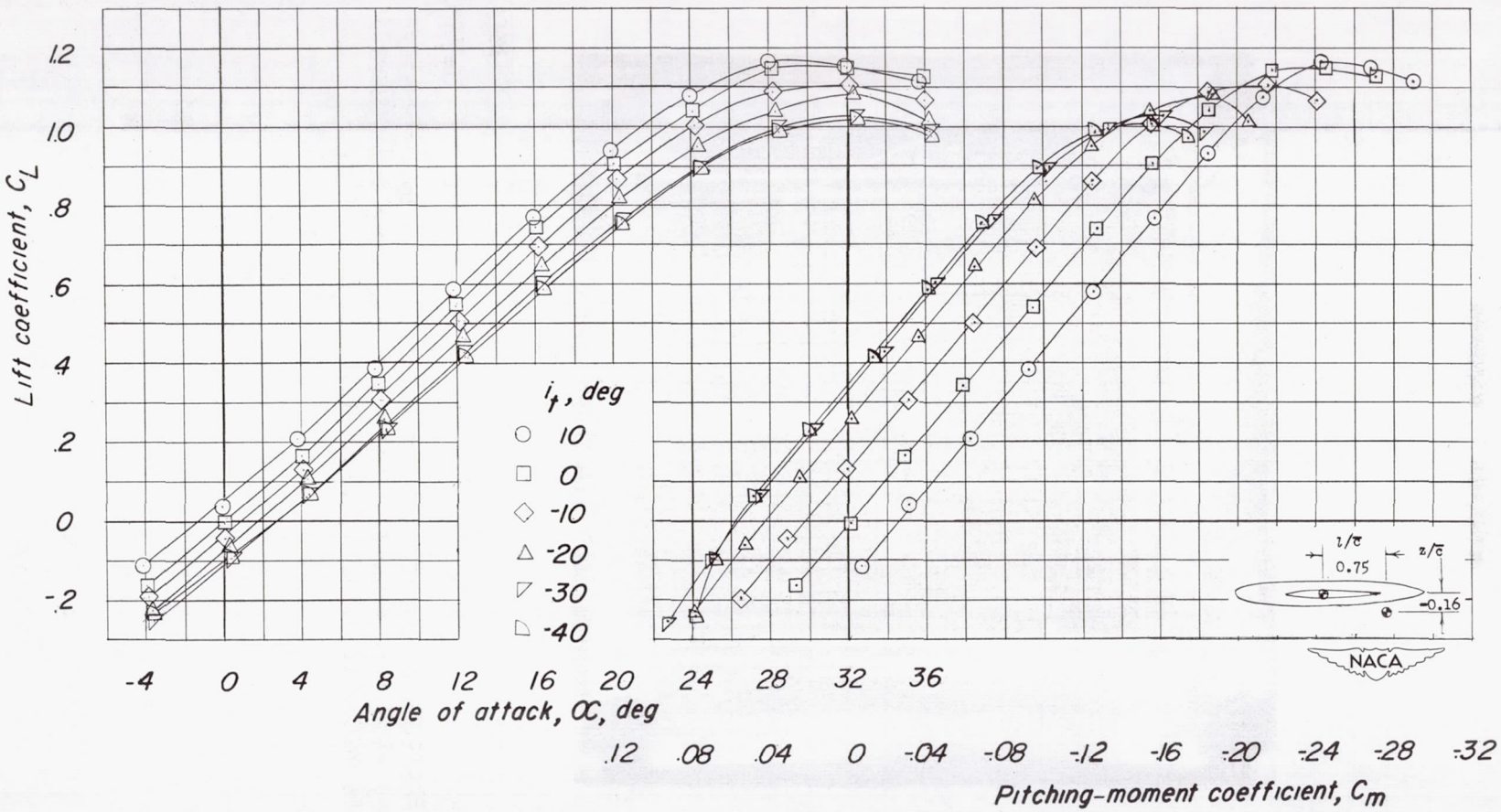

Figure 4.- Longitudinal stability and control characteristics of a 60° triangular-wing model having twin triangular all-movable tails. $2H_1$.

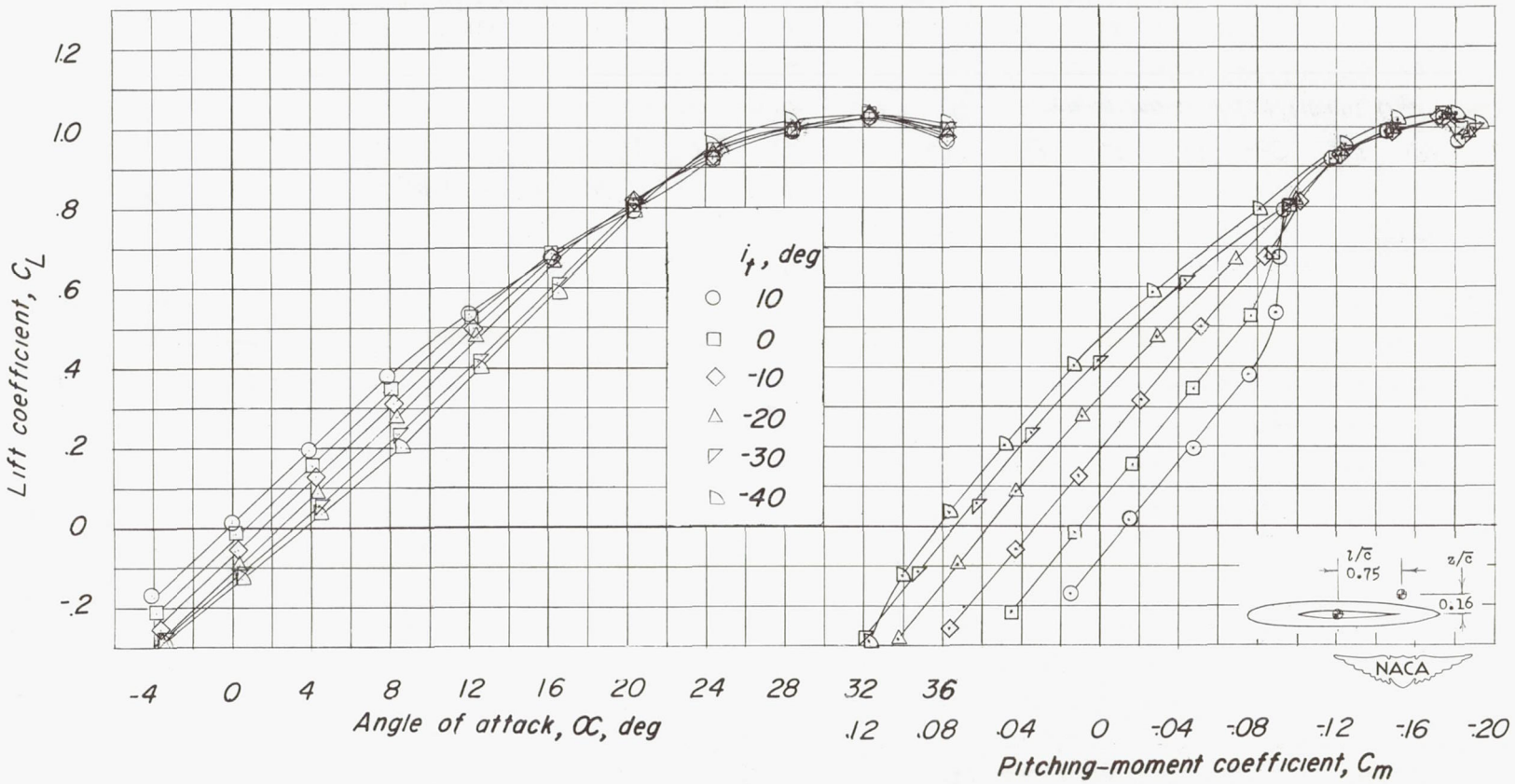

Figure 5.- Longitudinal stability and control characteristics of a 60° triangular-wing model having twin triangular all-movable tails. $2H_1$.

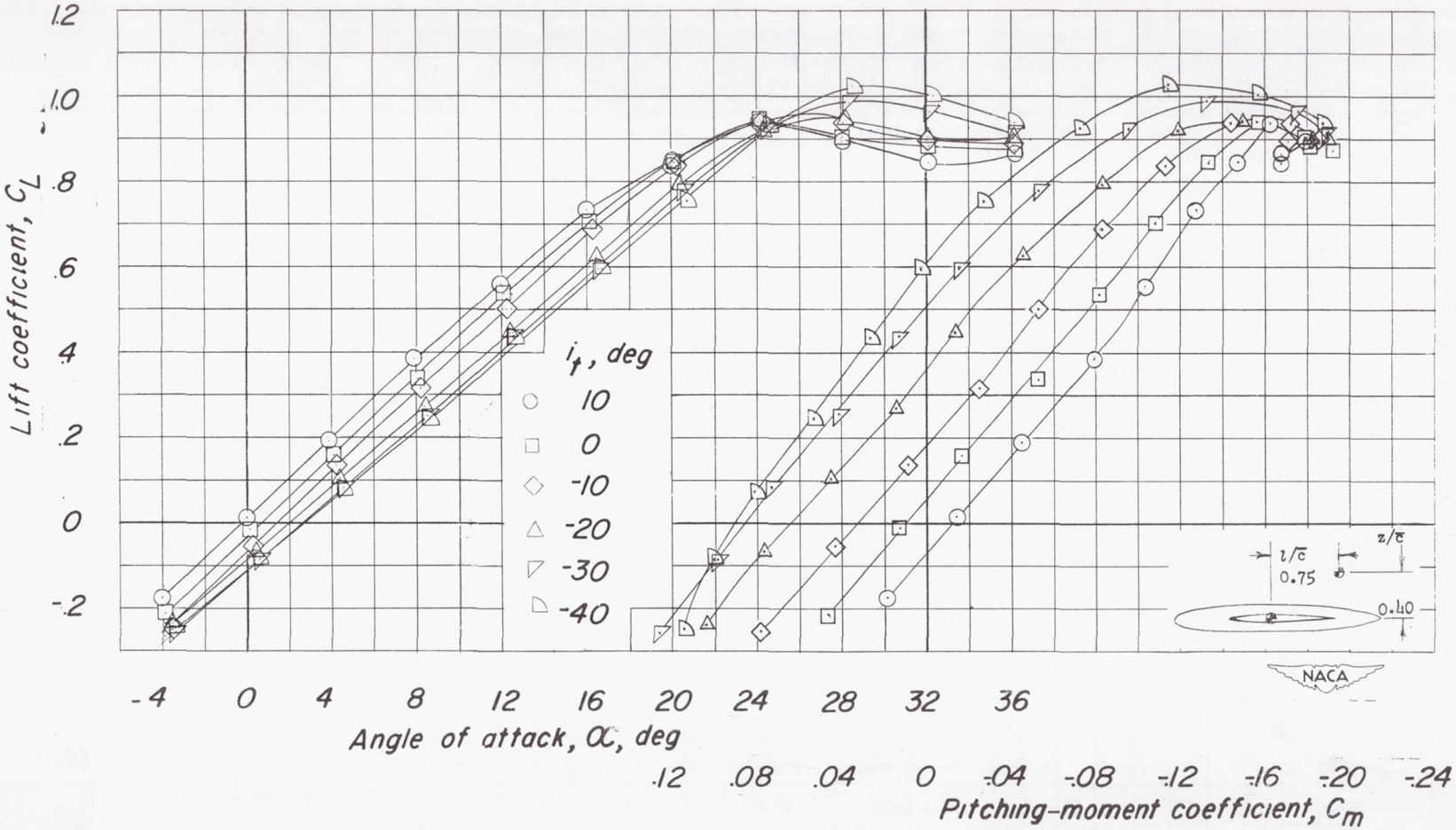

Figure 6.- Longitudinal stability and control characteristics of a 60° triangular-wing model having twin triangular all-movable tails. $2H_1$.

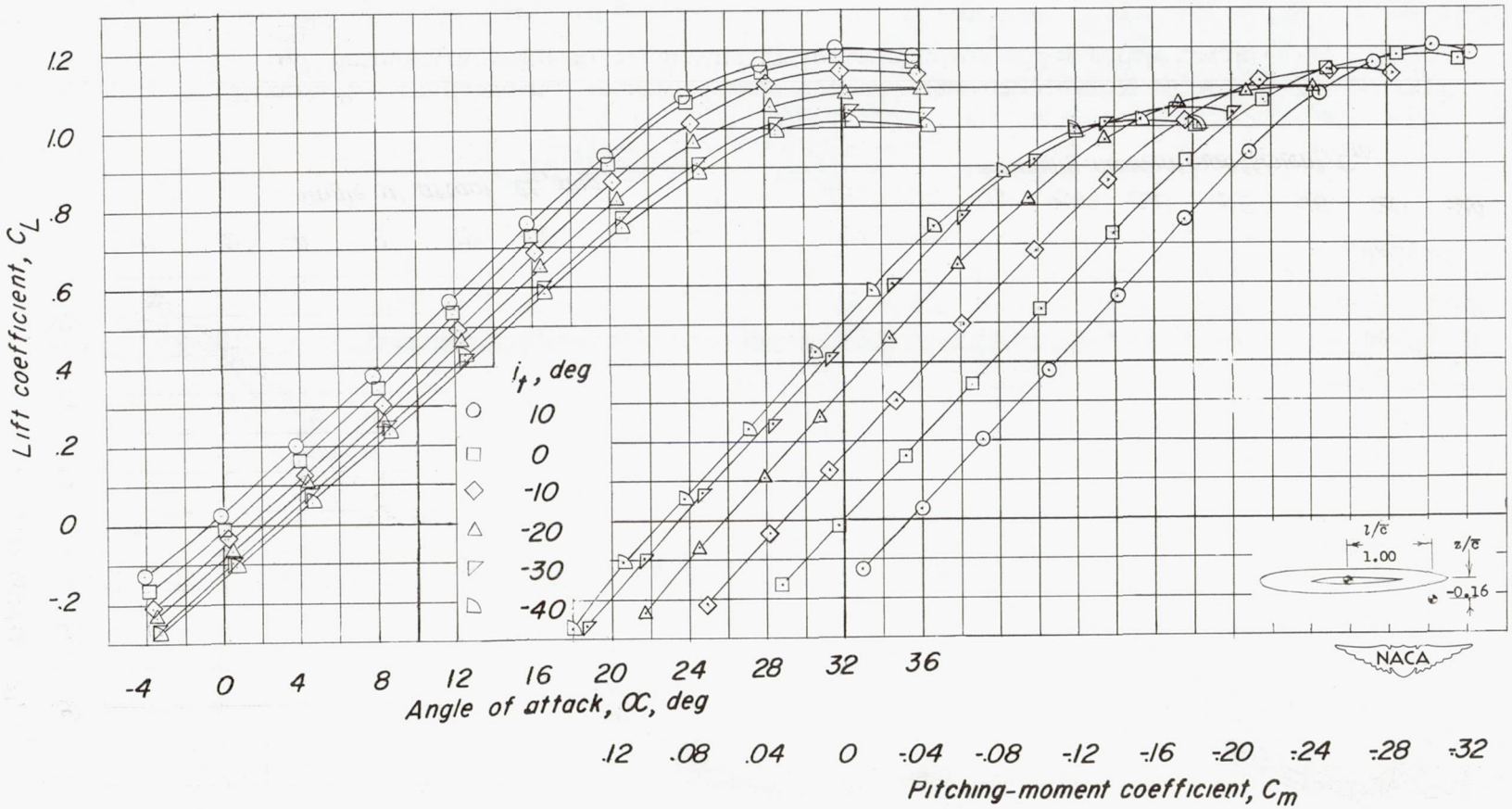

Figure 7.- Longitudinal stability and control characteristics of a 60° triangular-wing model having twin triangular all-movable tails. $2H_1$.

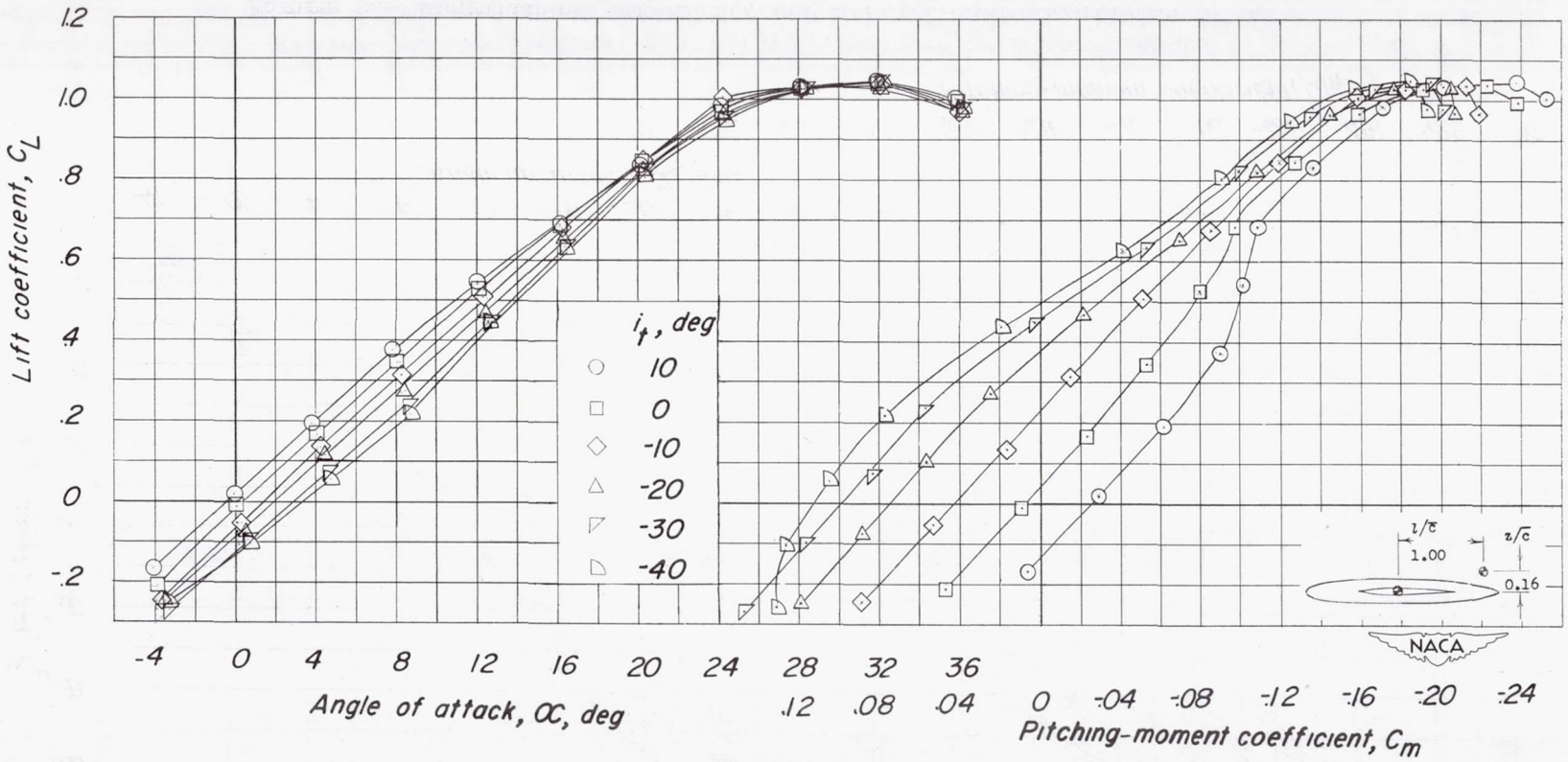

Figure 8.- Longitudinal stability and control characteristics of a 60° triangular-wing model having twin triangular all-movable tails. $2H_1$.

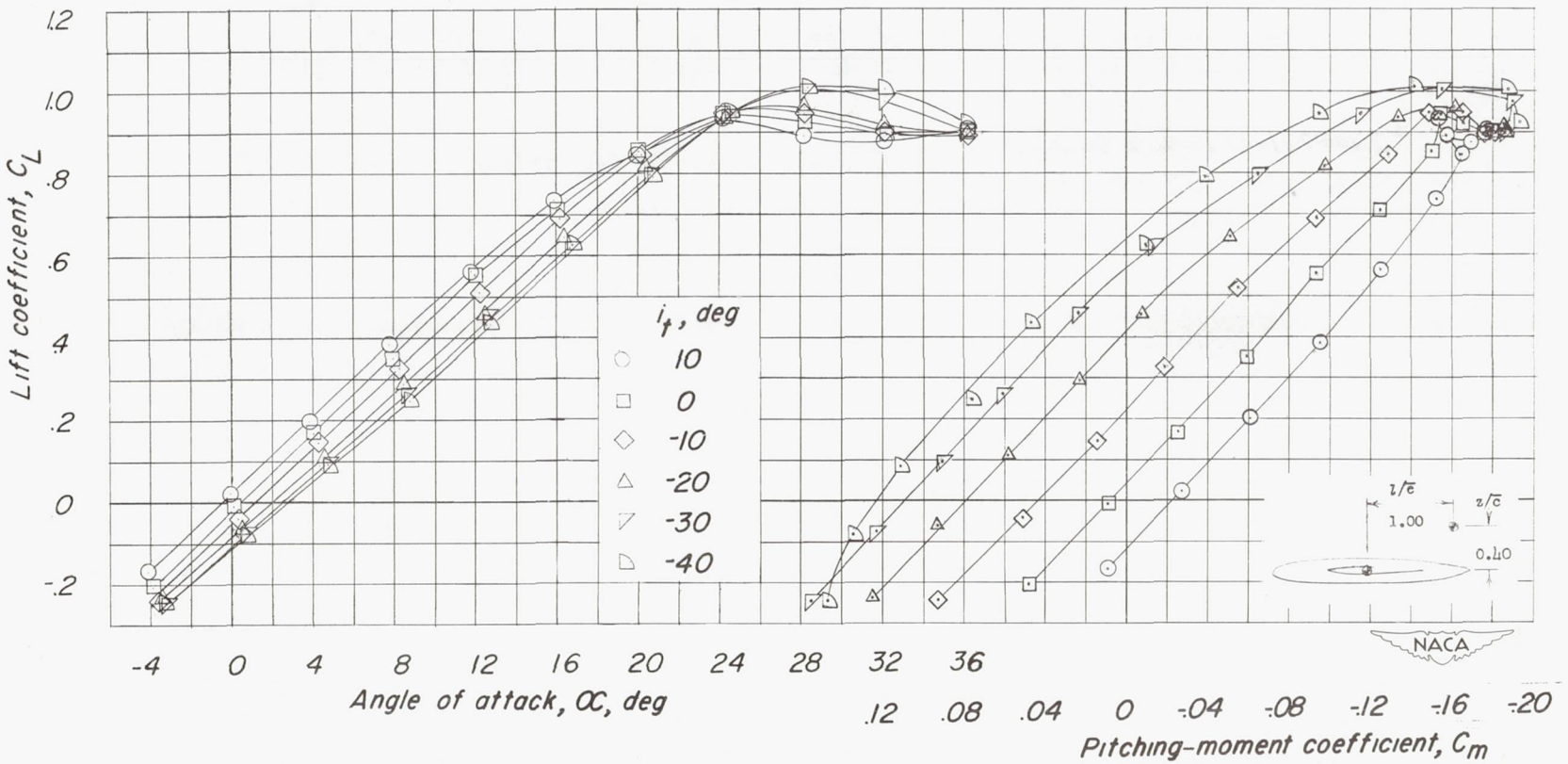

Figure 9.- Longitudinal stability and control characteristics of a 60° triangular-wing model having twin triangular all-movable tails. $2H_1$.

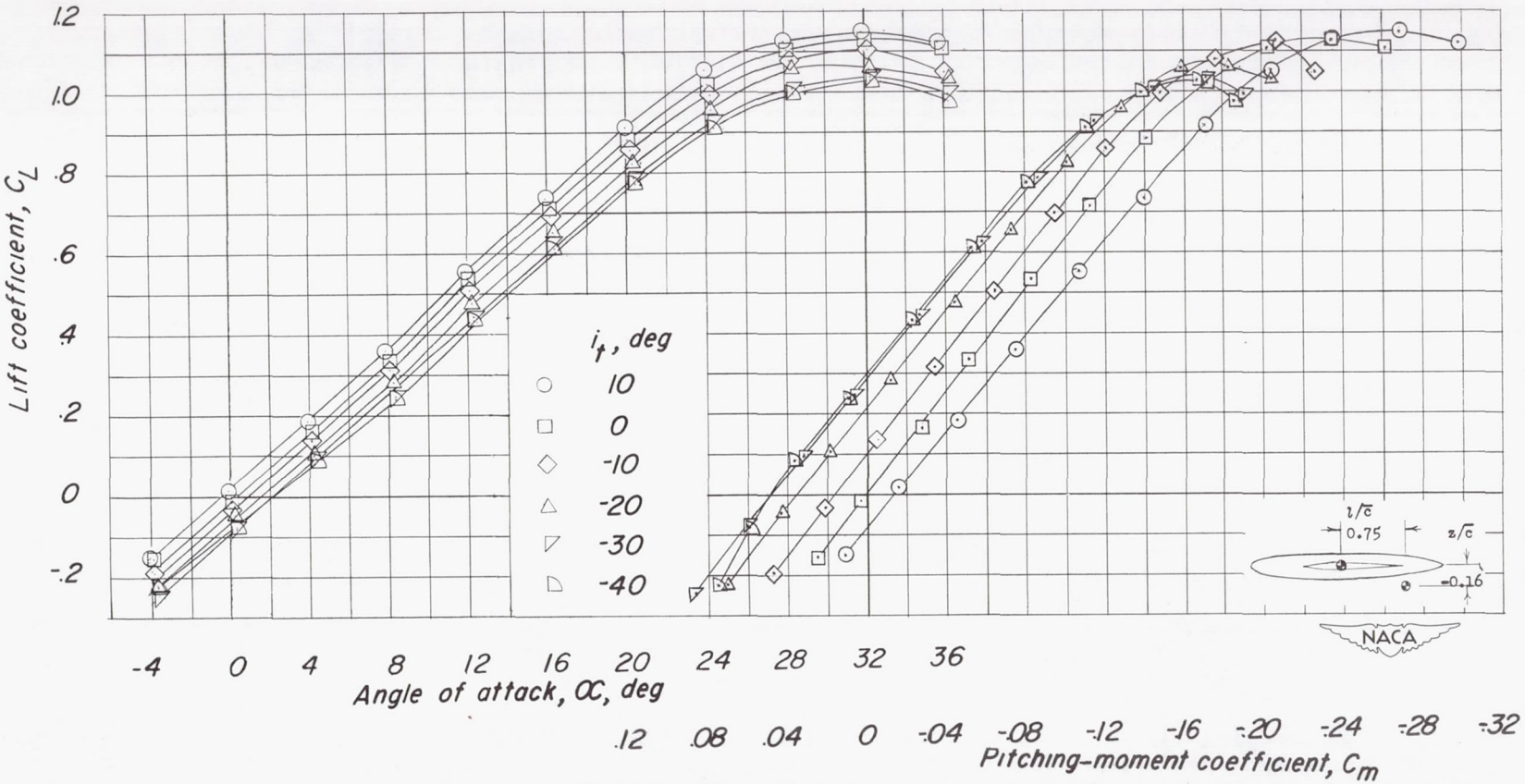

Figure 10.- Longitudinal stability and control characteristics of a 60° triangular-wing model having twin triangular all-movable tails. $2H_2$.

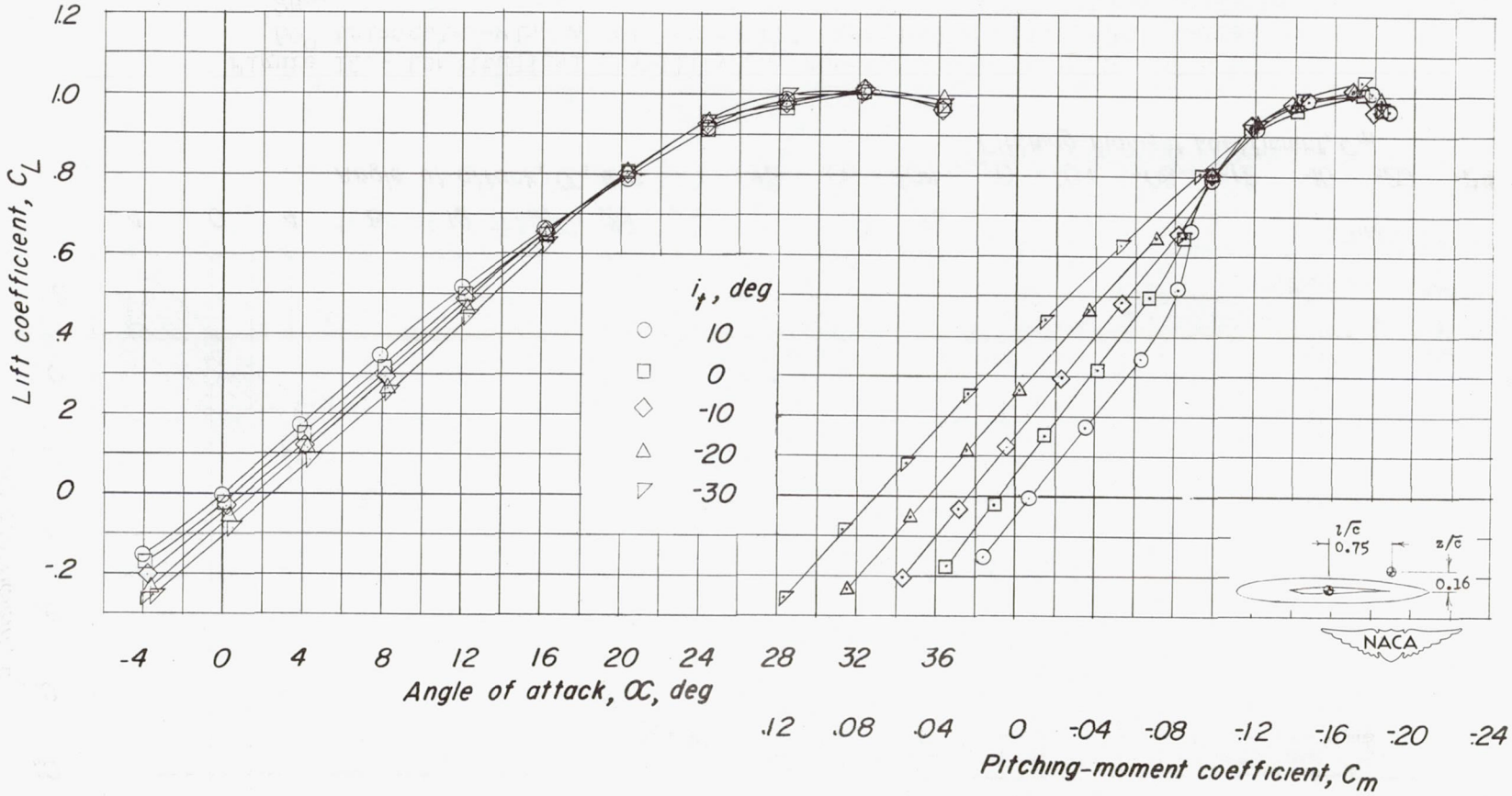

Figure 11.- Longitudinal stability and control characteristics of a 60° triangular-wing model having twin triangular all-movable tails. $2H_2$.

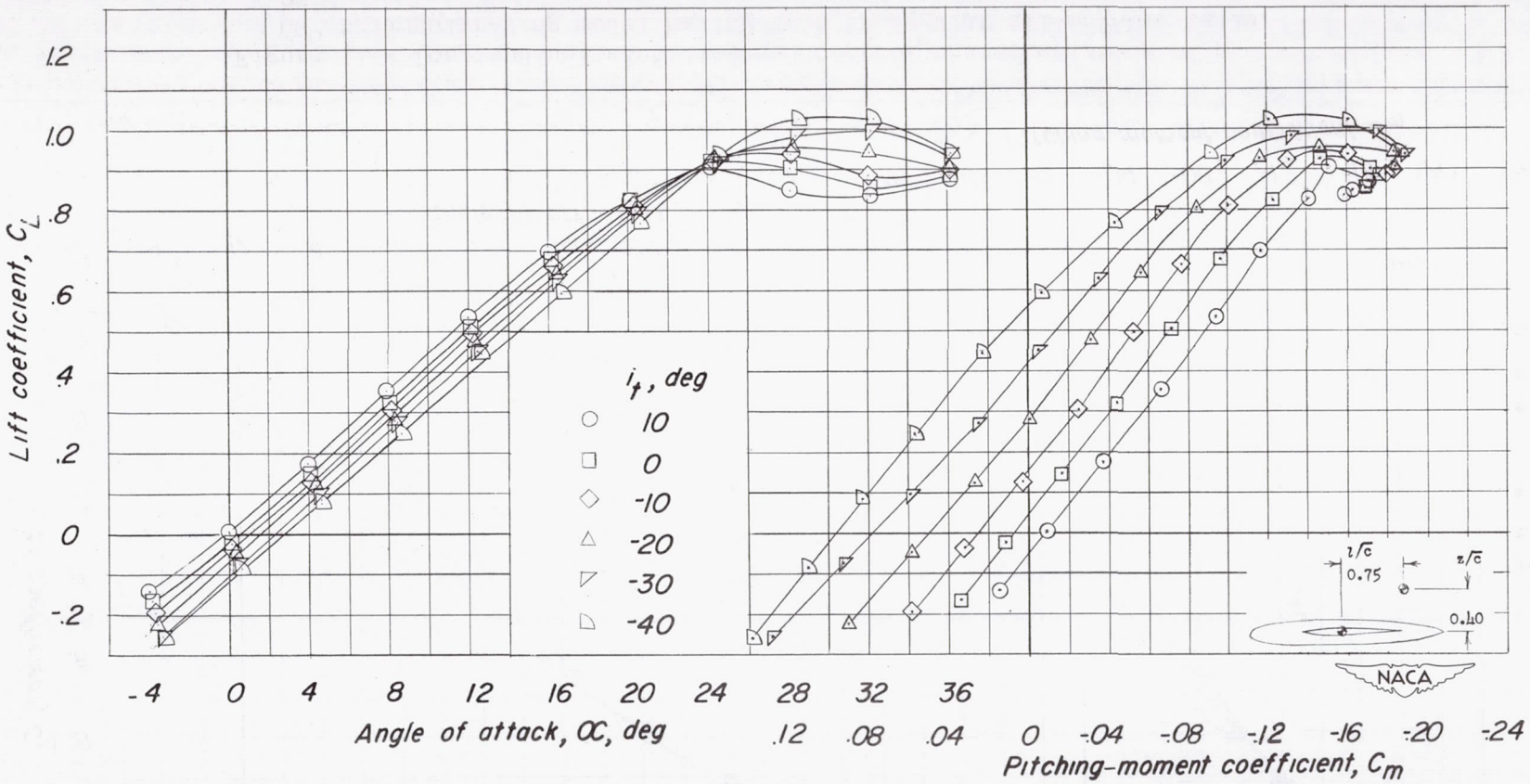

Figure 12.- Longitudinal stability and control characteristics of a 60° triangular-wing model having twin triangular all-movable tails. $2H_2$.

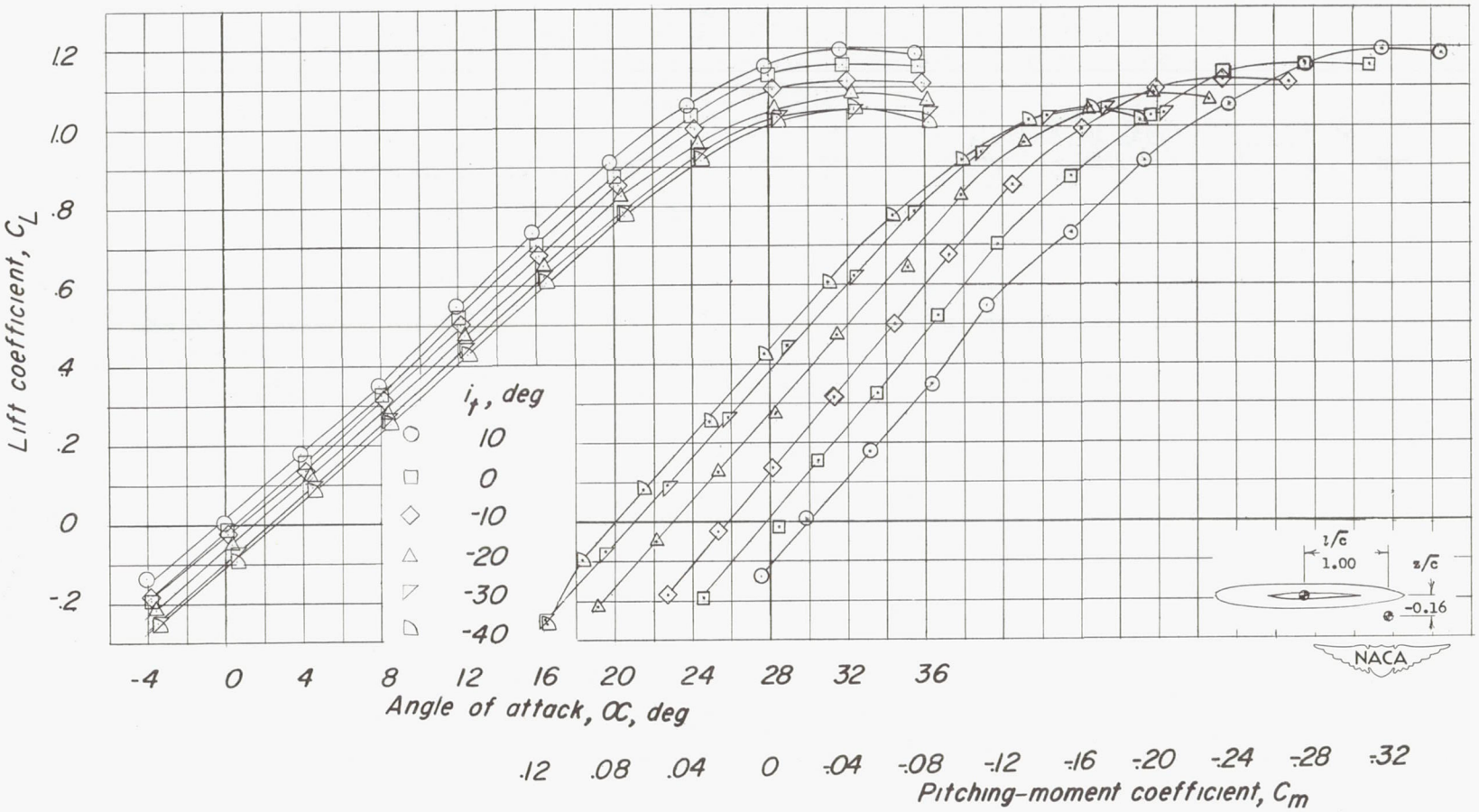

Figure 13.- Longitudinal stability and control characteristics of a 60° triangular-wing model having twin triangular all-movable tails. $2H_2$.

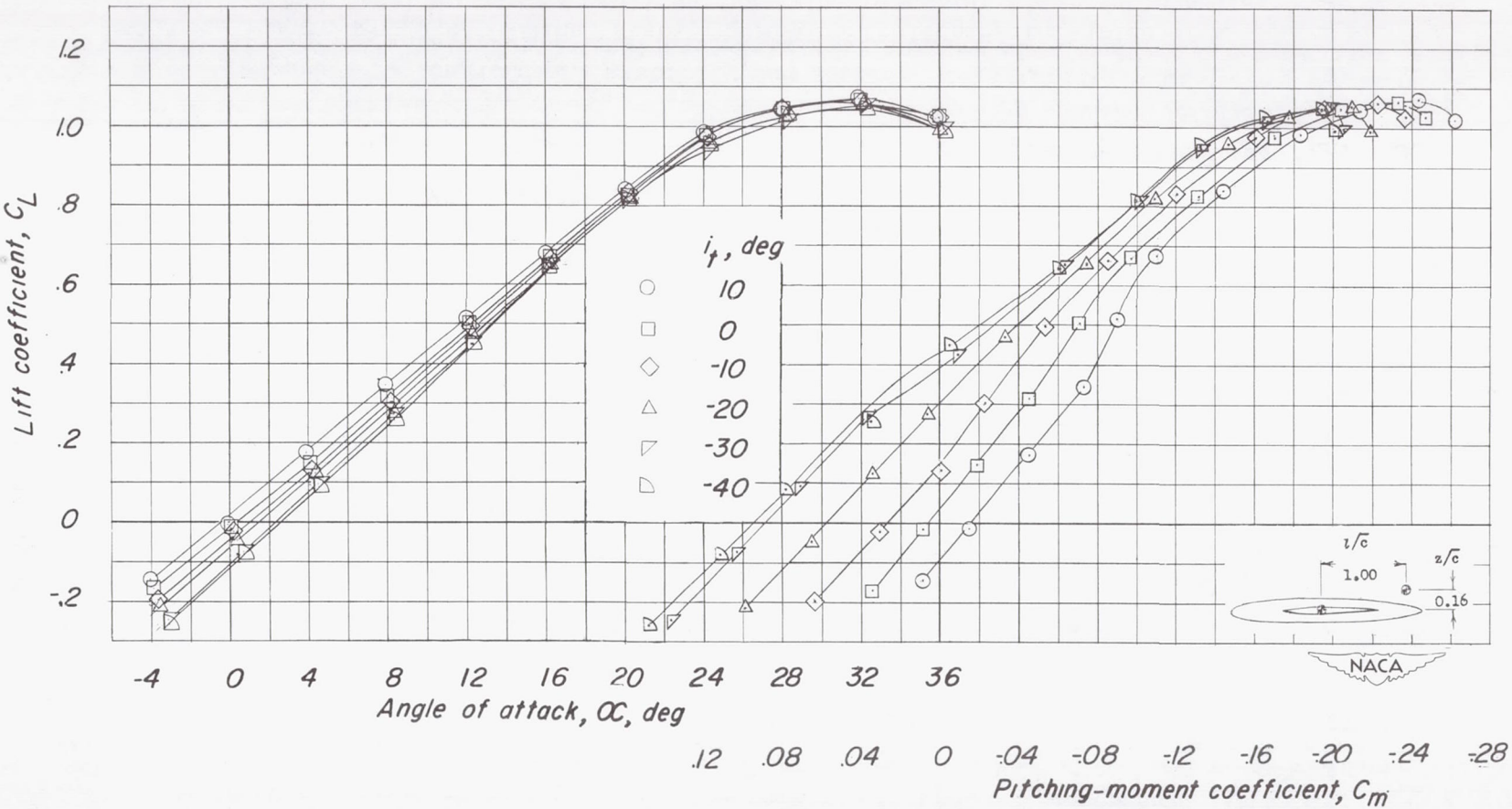

Figure 14.- Longitudinal stability and control characteristics of a 60° triangular-wing model having twin triangular all-movable tails. $2H_2$.

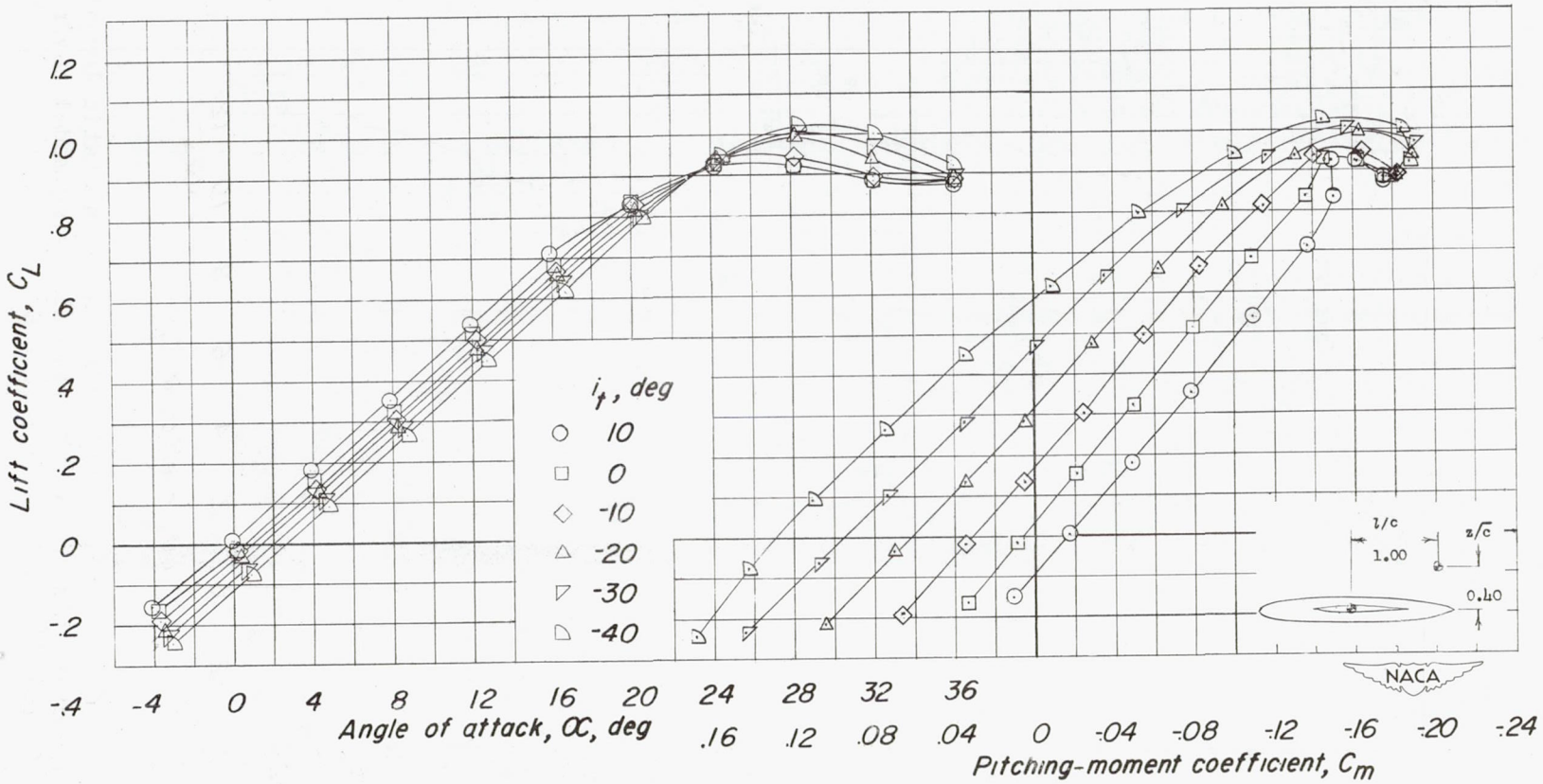

Figure 15.- Longitudinal stability and control characteristics of a 60° triangular-wing model having twin triangular all-movable tails. $2H_2$.

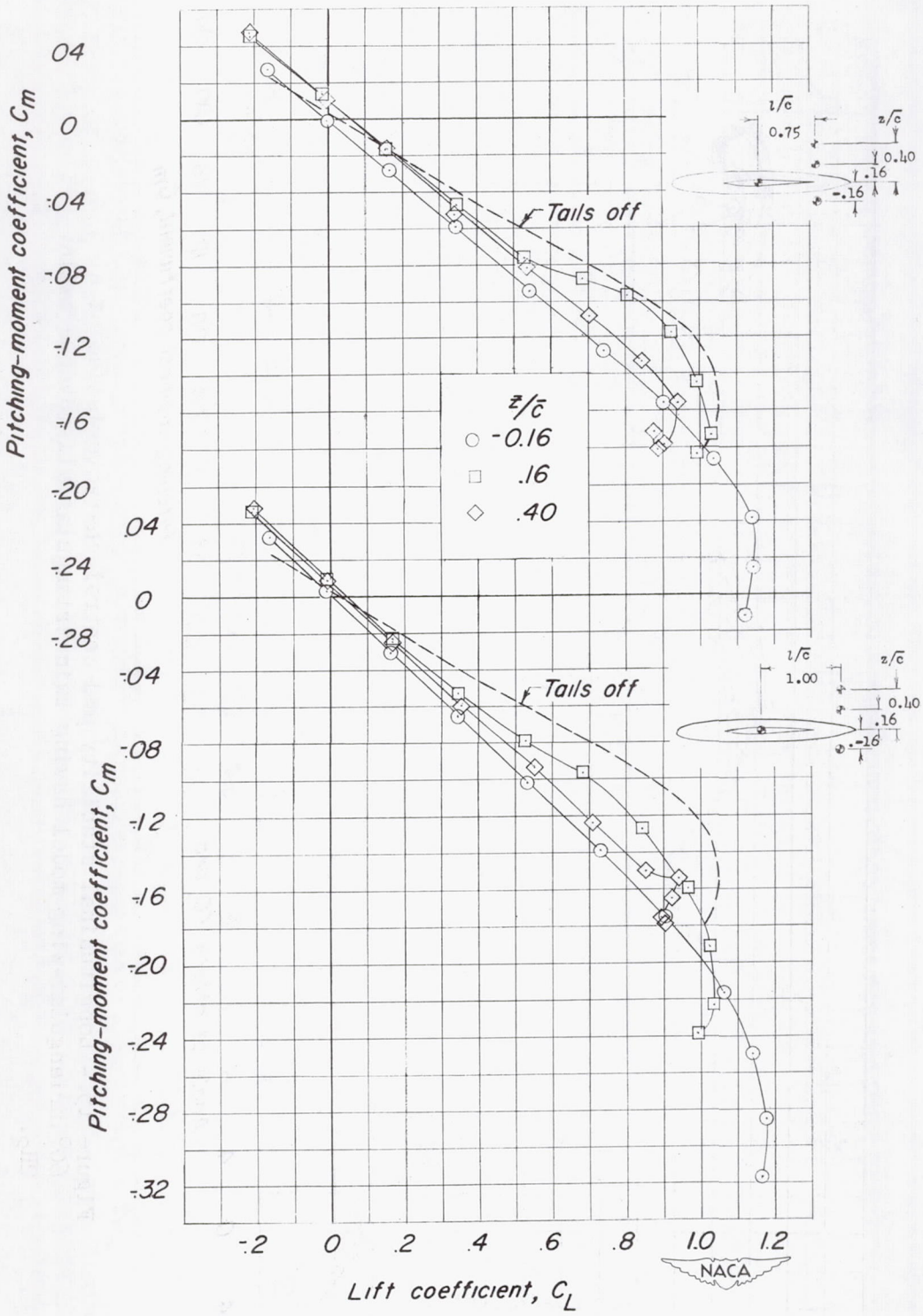

Figure 16.- Effect of tail height and tail length on static longitudinal stability characteristics of a 60° triangular-wing model having twin triangular all-movable tails. $2H_1$; $i_t = 0^\circ$.

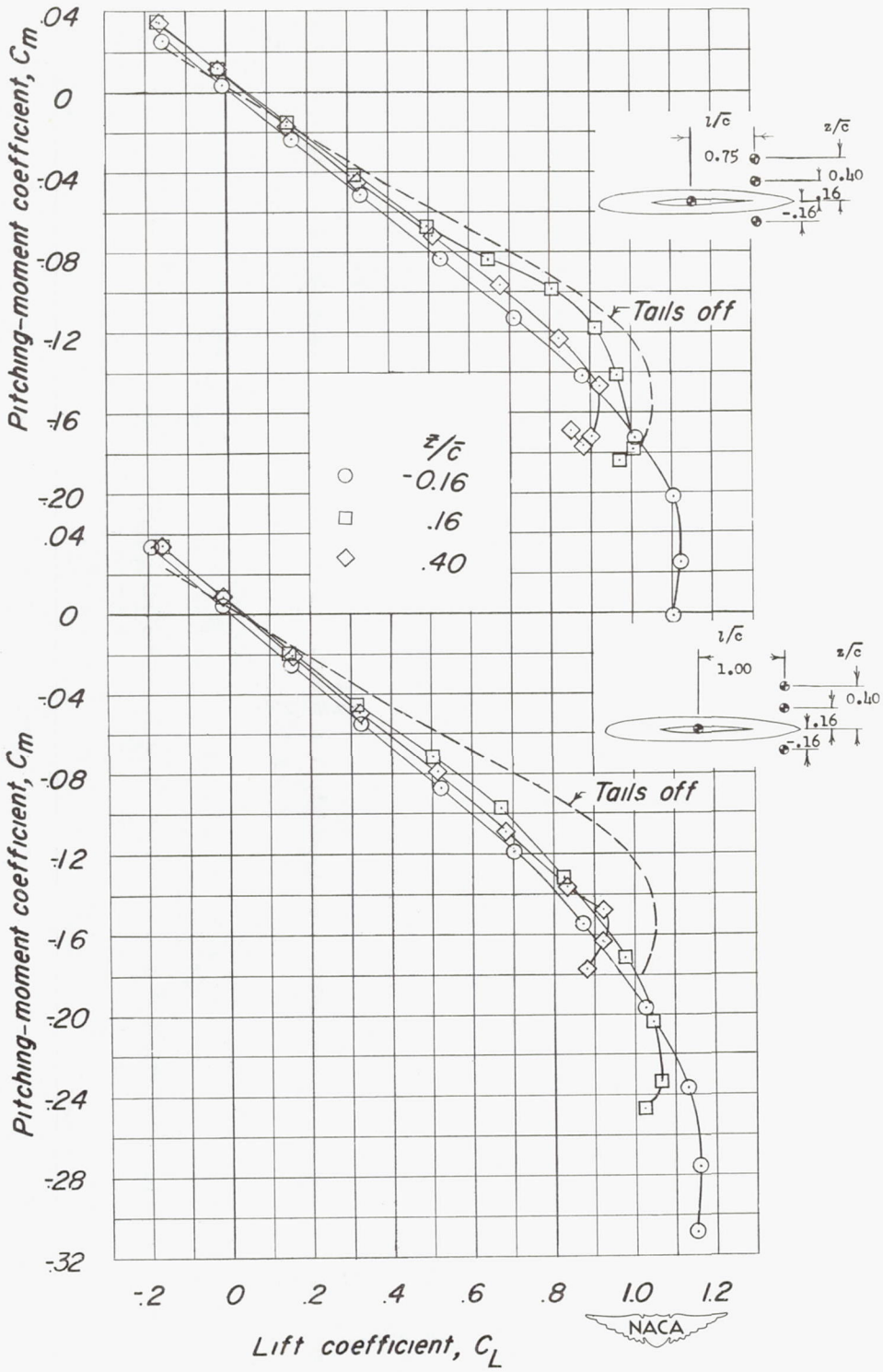

Figure 17.- Effect of tail height and tail length on static longitudinal stability characteristics of a 60° triangular-wing model having twin triangular all-movable tails. $2H_2$; $i_t = 0°$.

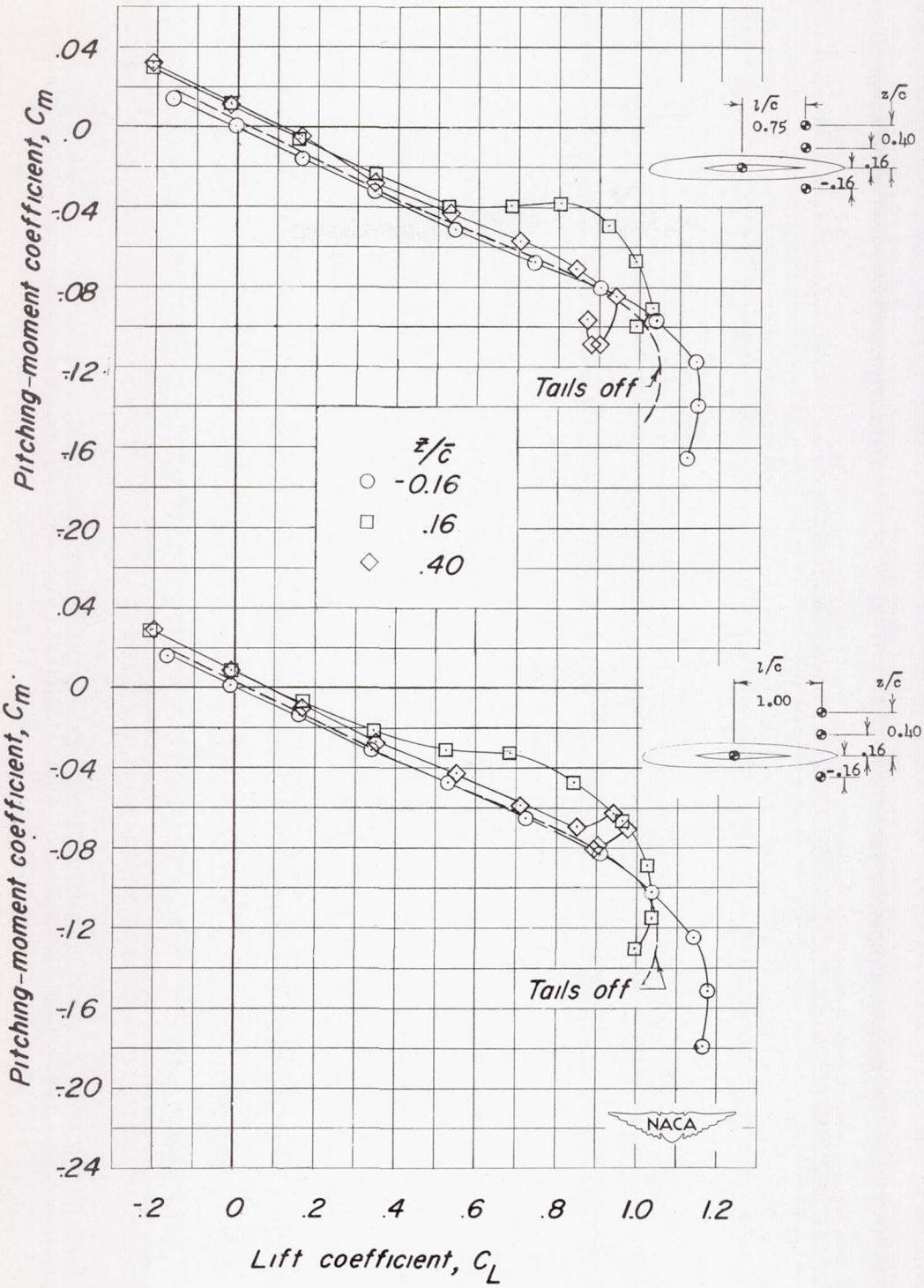

Figure 18.- Effect of tail height and tail length on static longitudinal stability characteristics of a 60° triangular-wing model having twin triangular all-movable tails. $2H_1$; $i_t = 0^\circ$; $C_{m_{C_L}} = -0.10$.

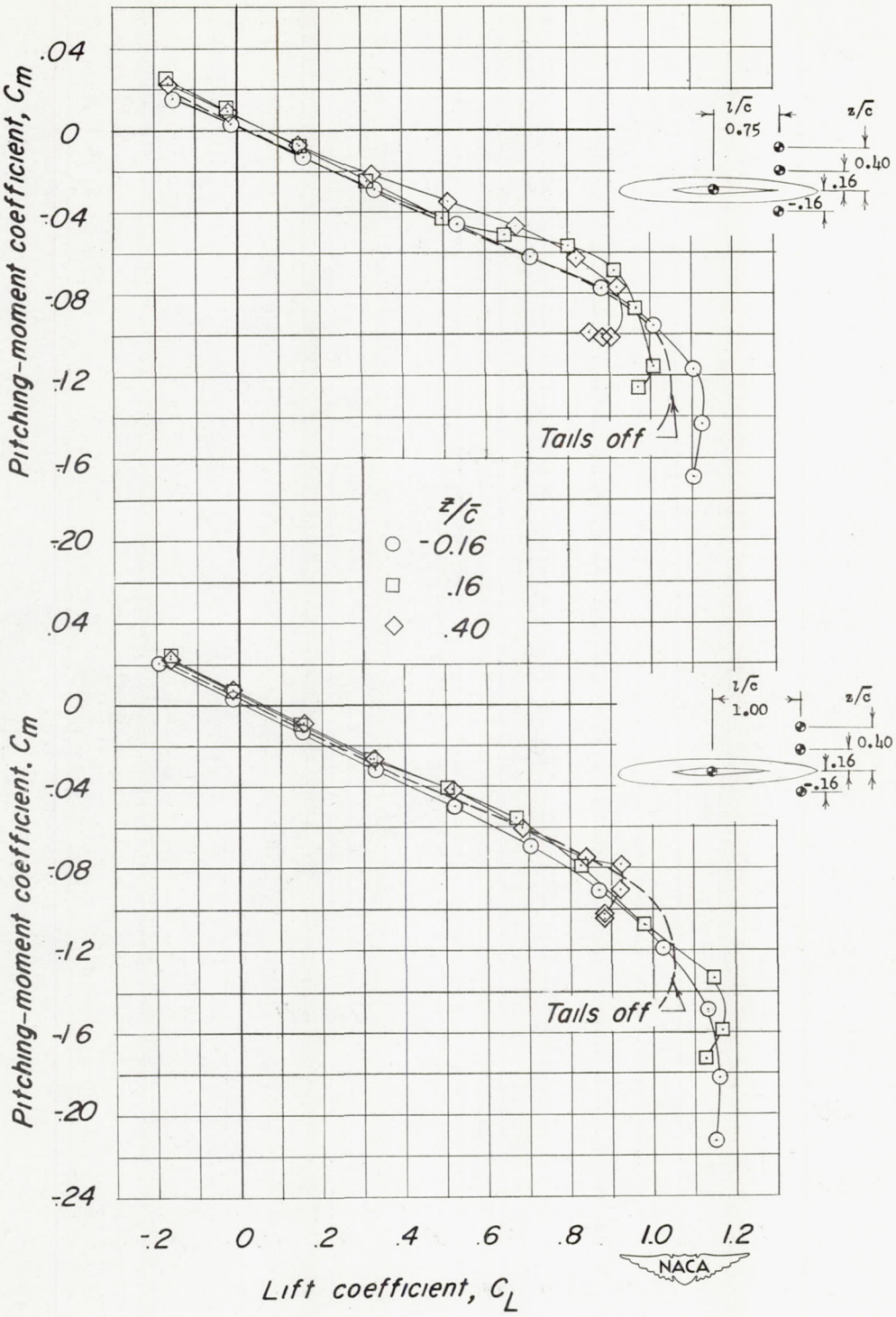

Figure 19.- Effect of tail height and tail length on static longitudinal stability characteristics of a 60° triangular-wing model having twin triangular all-movable tails. $2H_2$; $i_t = 0^\circ$; $C_{m_{C_L}} = -0.10$.

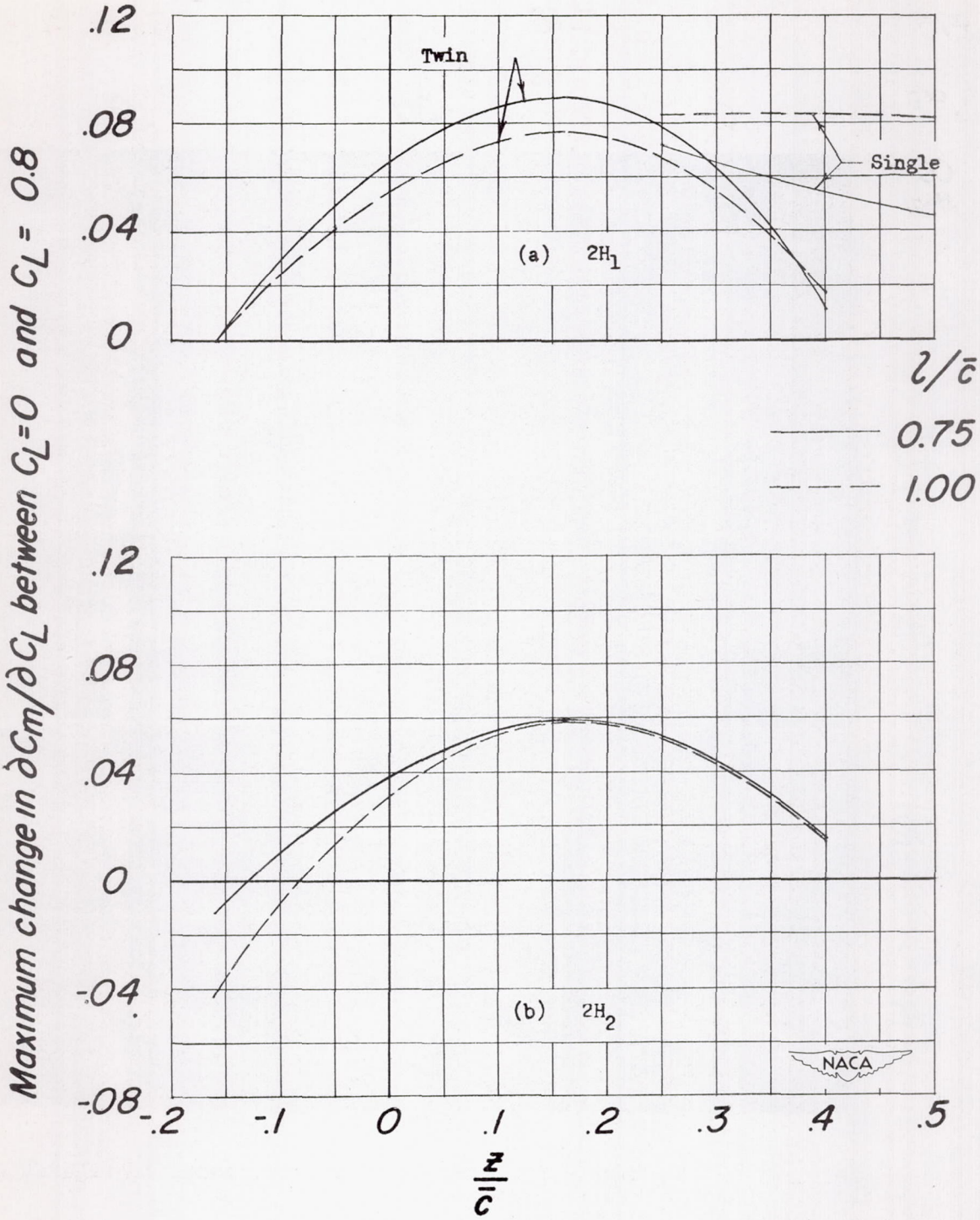

Figure 20.- Summary of effect of tail location on static longitudinal stability. $i_t = 0^{\circ}$; $\frac{2S_H}{S} = 0.10$.

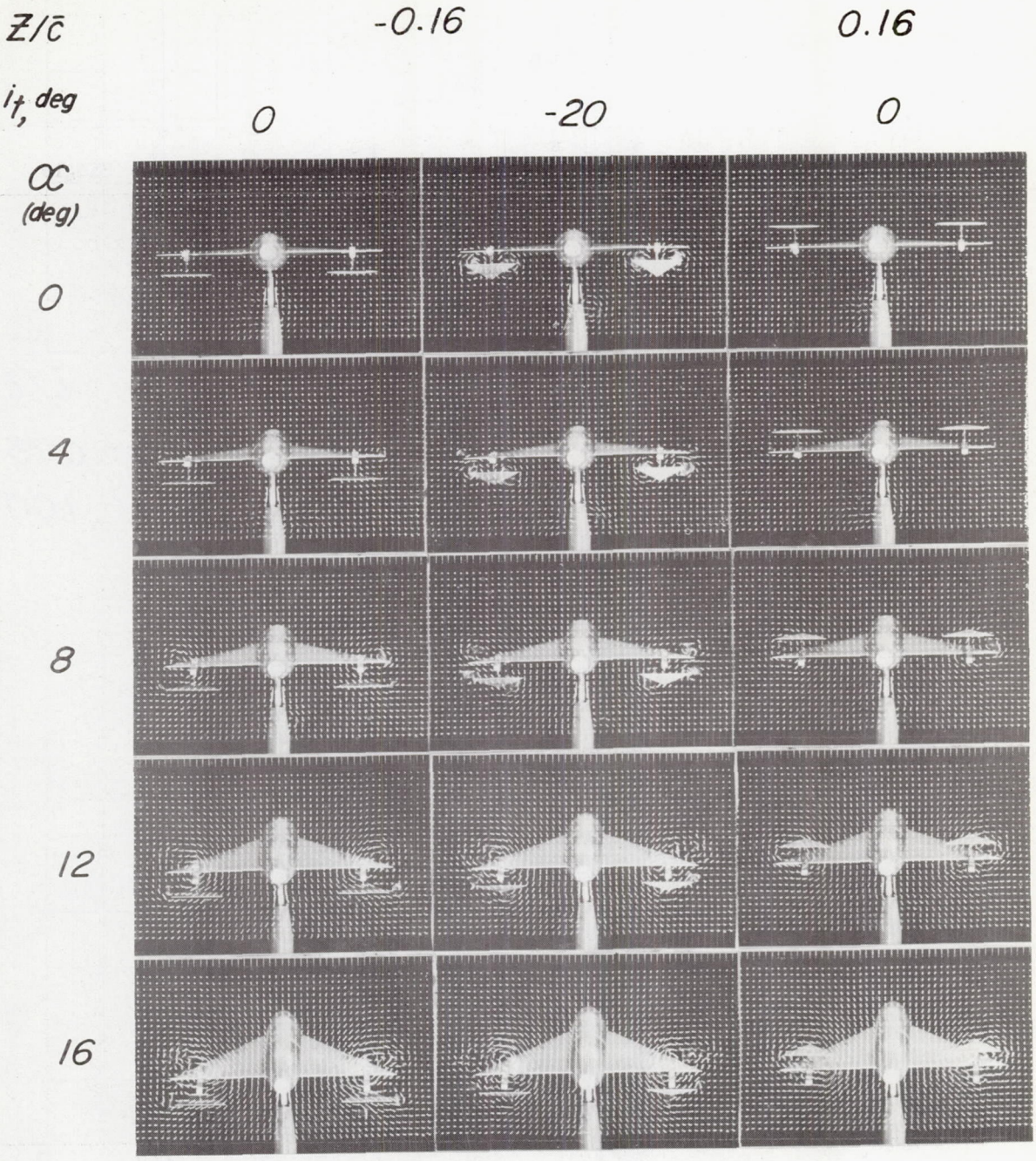

Figure 21.- Tuft-grid photographs of several model configurations. $R = 0.92 \times 10^6$; $\frac{l}{\bar{c}} = 0.75$; $2H_1$.

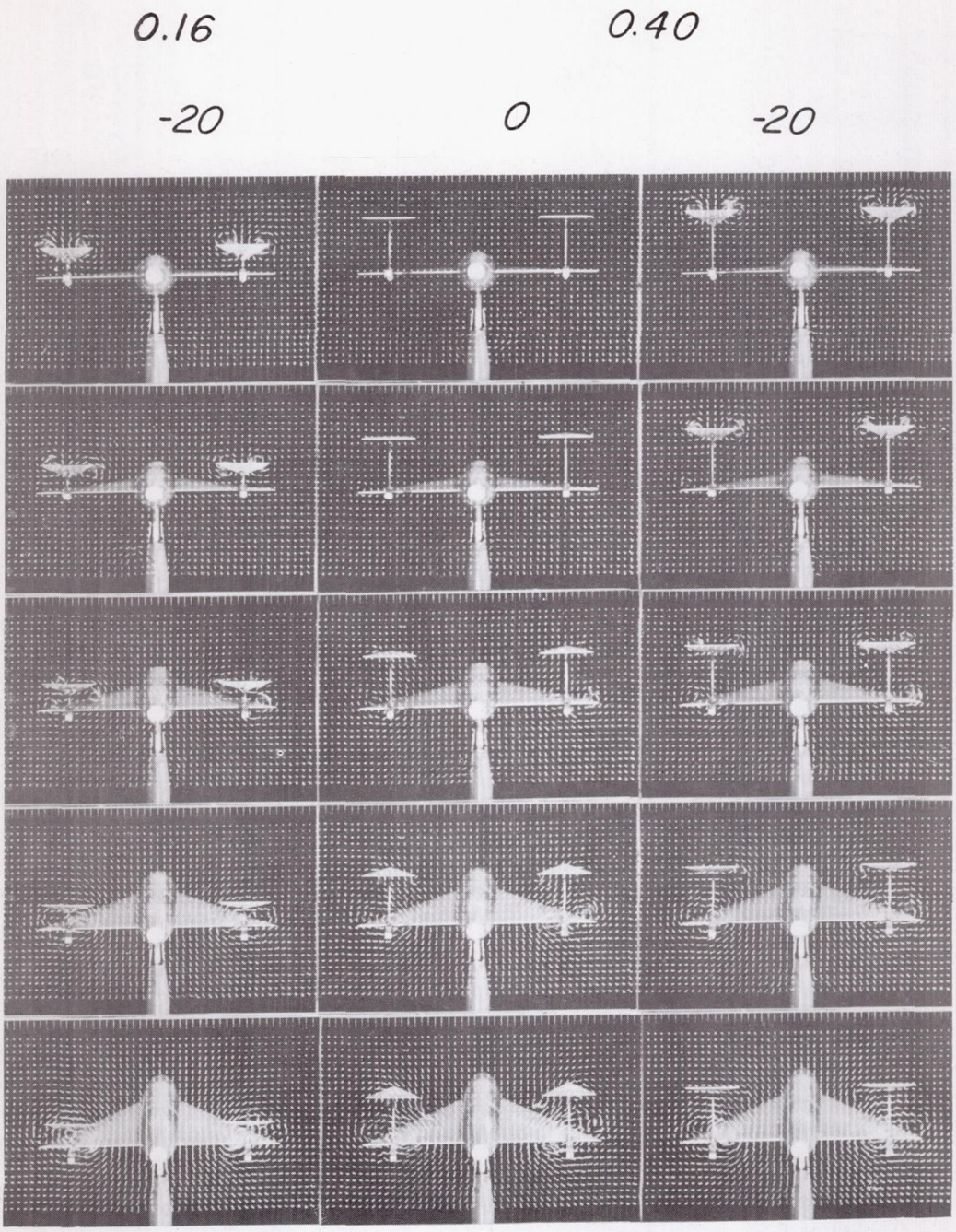

Figure 21.- Continued. L-72746

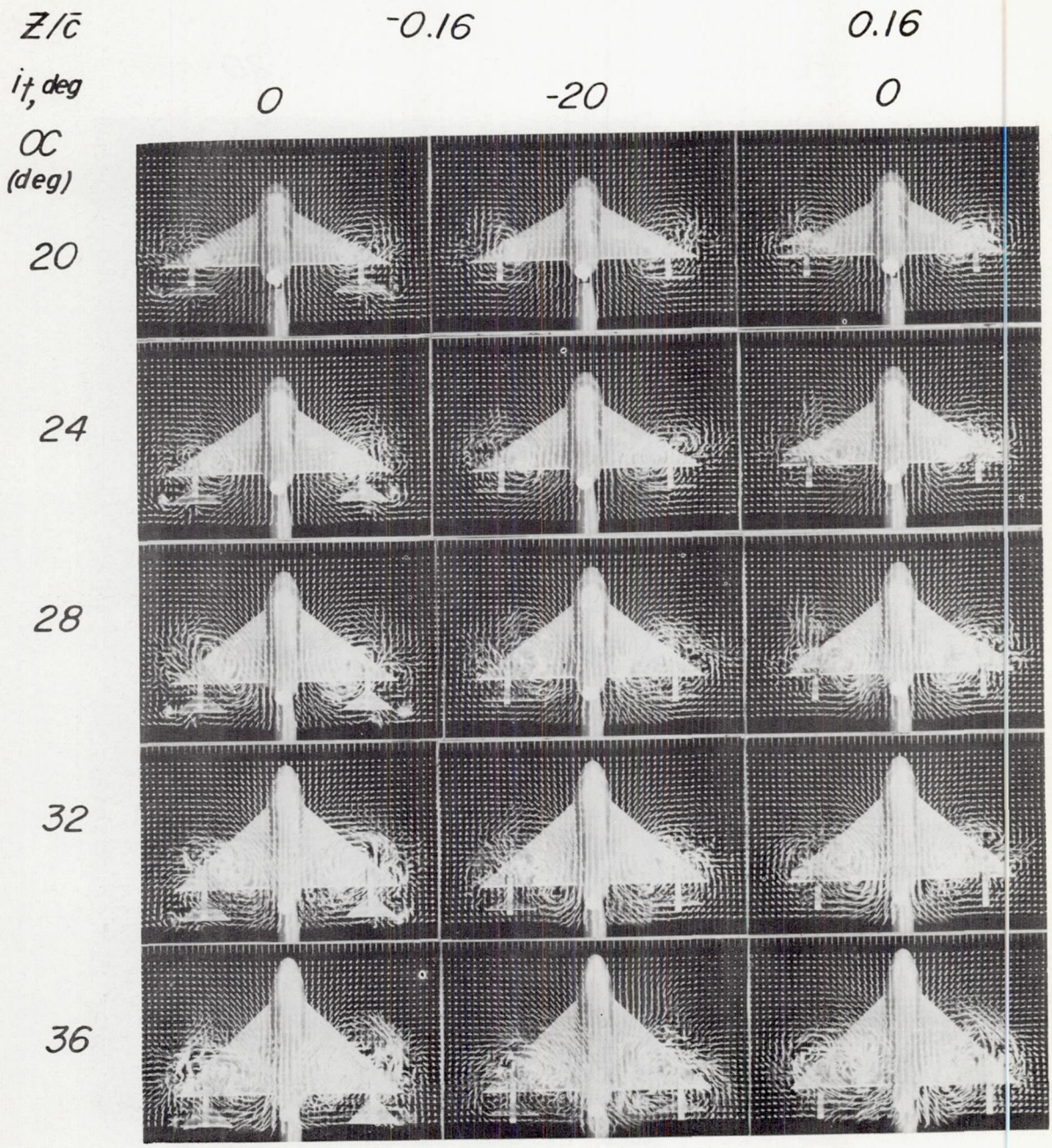

Figure 21.- Continued.

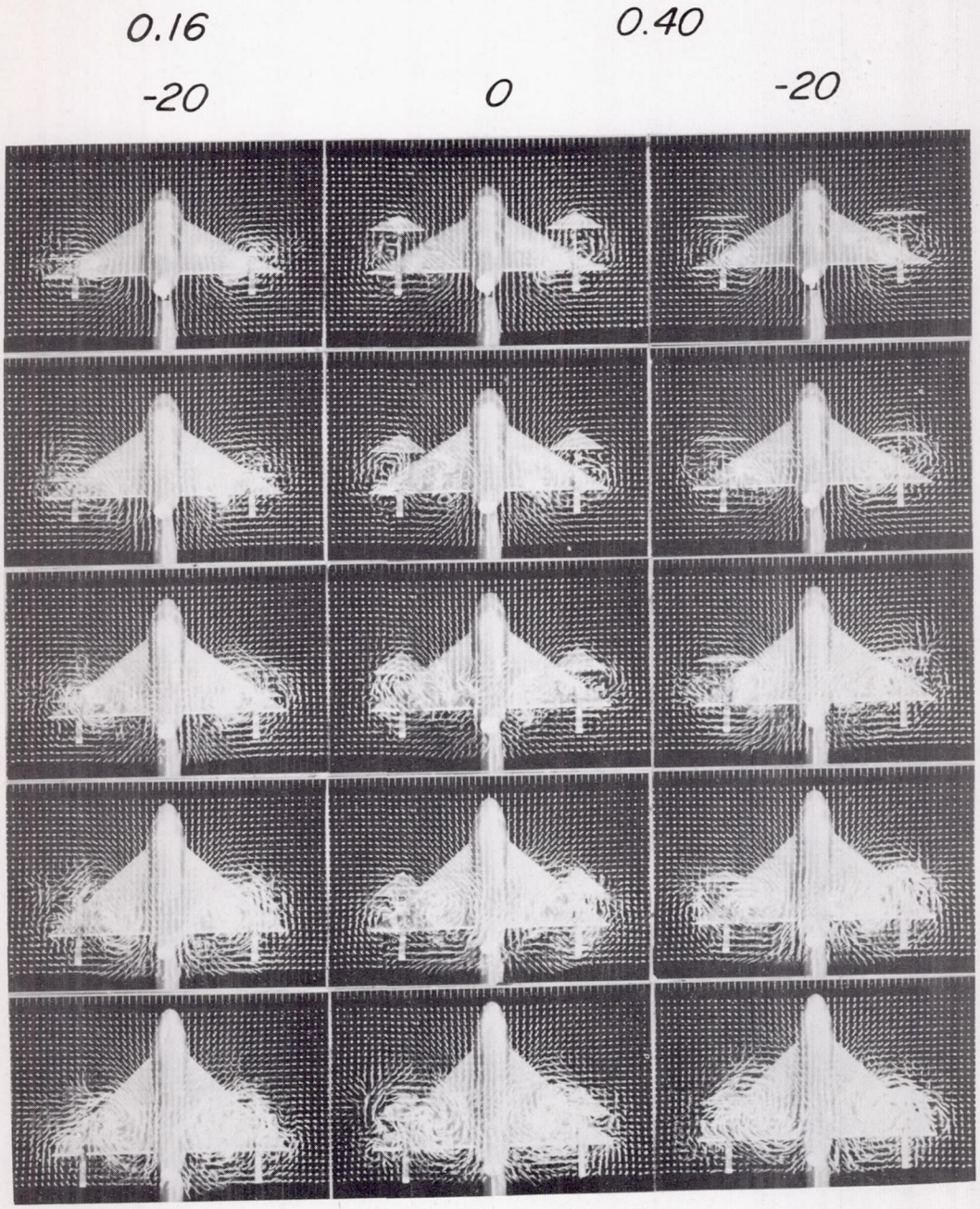

Figure 21.- Concluded. L-72747

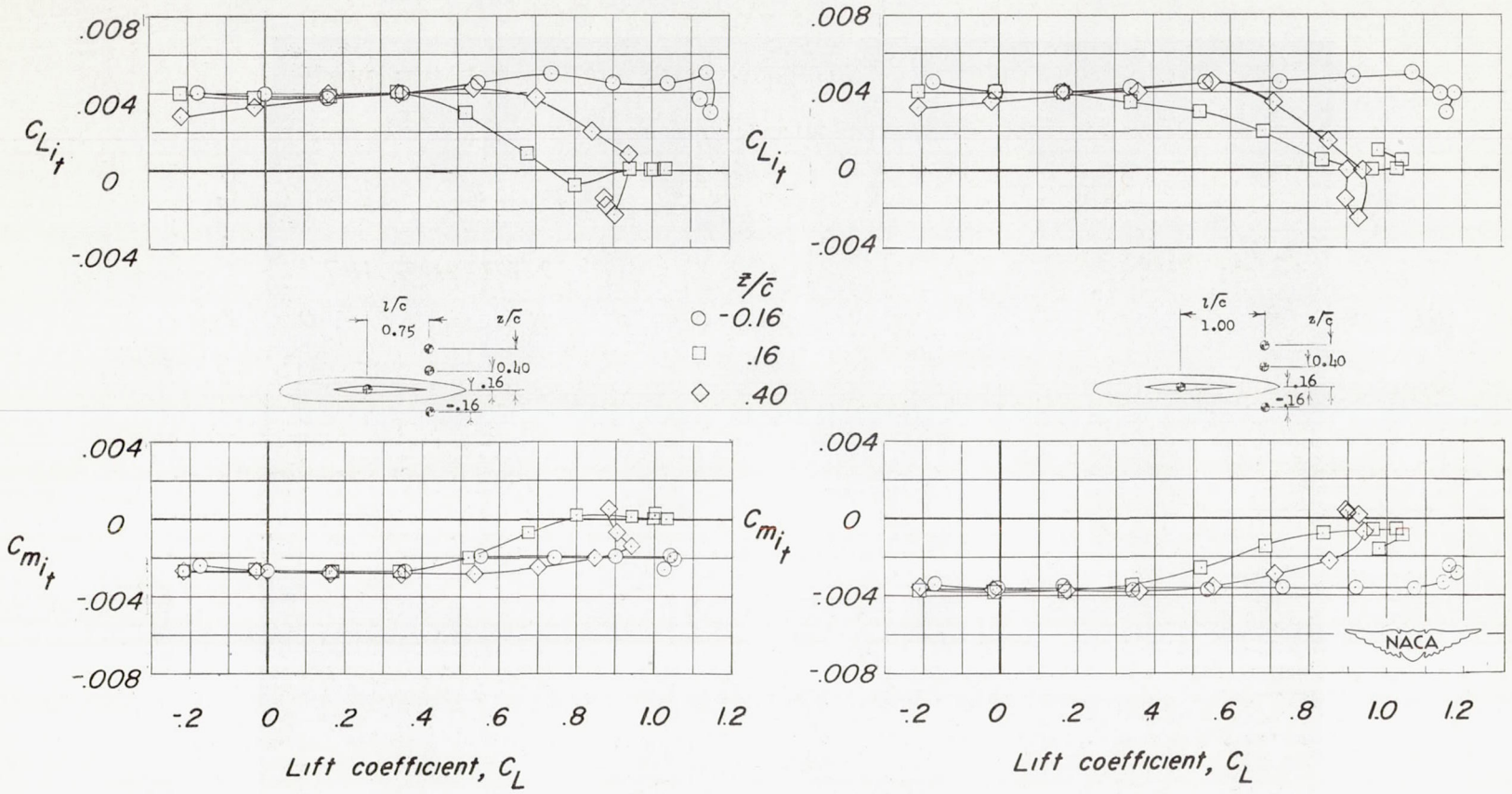

Figure 22.- Effect of tail height and tail length on variation of $C_{L_{i_t}}$ and $C_{m_{i_t}}$ with C_L for a 60° triangular wing model having twin triangular all-movable tails. $2H_1$. $C_{m_{C_L}} = -0.10$ at $C_L = 0$. (See text for centers of gravity.)

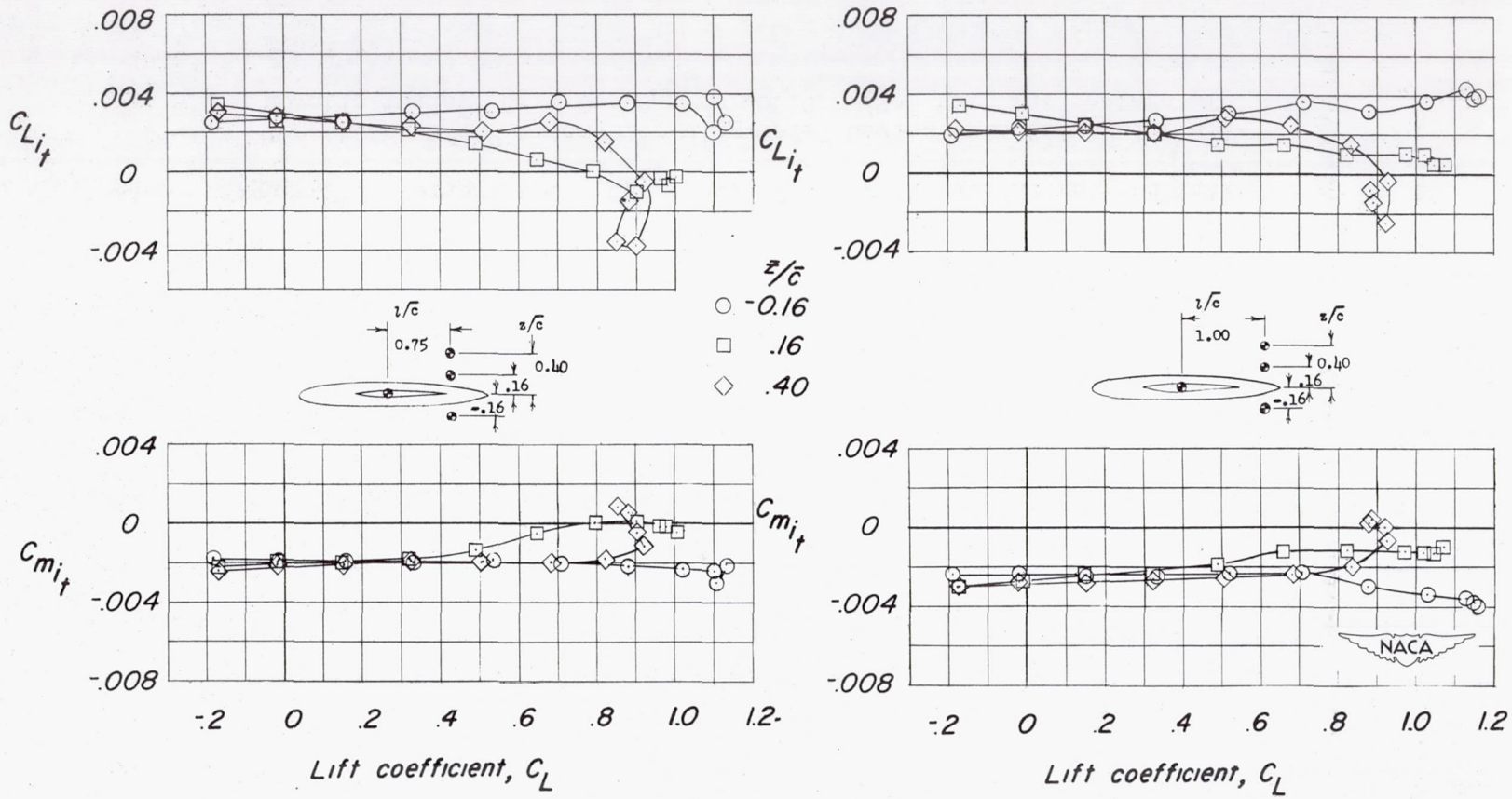

Figure 23.- Effect of tail height and tail length on variation of $C_{L_{i_t}}$ and $C_{m_{i_t}}$ with C_L for a 60° triangular-wing model having twin triangular all-movable tails. $2H_2$. $C_{m_{C_L}} = -0.10$ at $C_L = 0$. (See text for centers of gravity.)

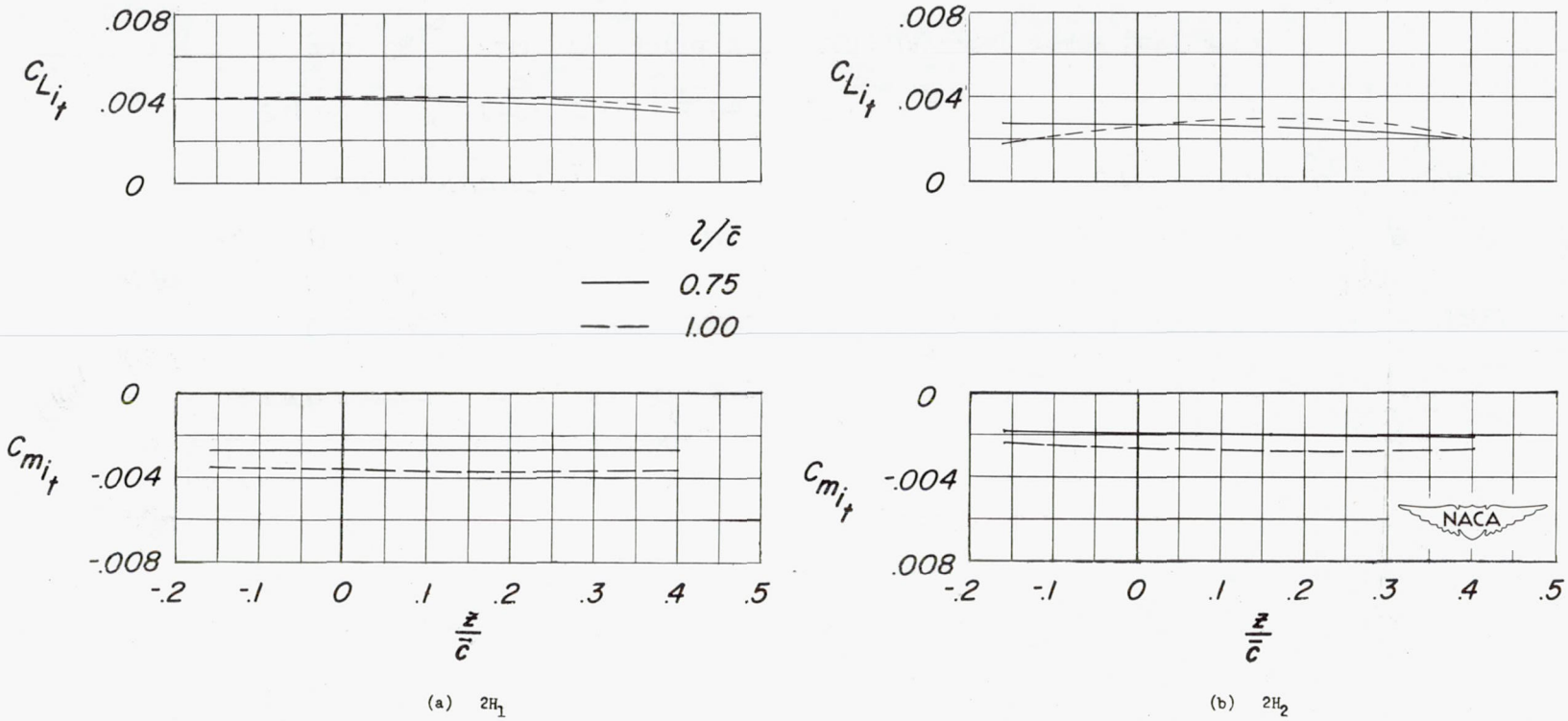

Figure 24.- Variation of $C_{L_{i_t}}$ and $C_{m_{i_t}}$ with tail height and tail length for a 60° triangular-wing model having twin triangular all-movable tails. $C_L = 0$. $C_{m_{C_L}} = -0.10$. (See text for centers of gravity.)

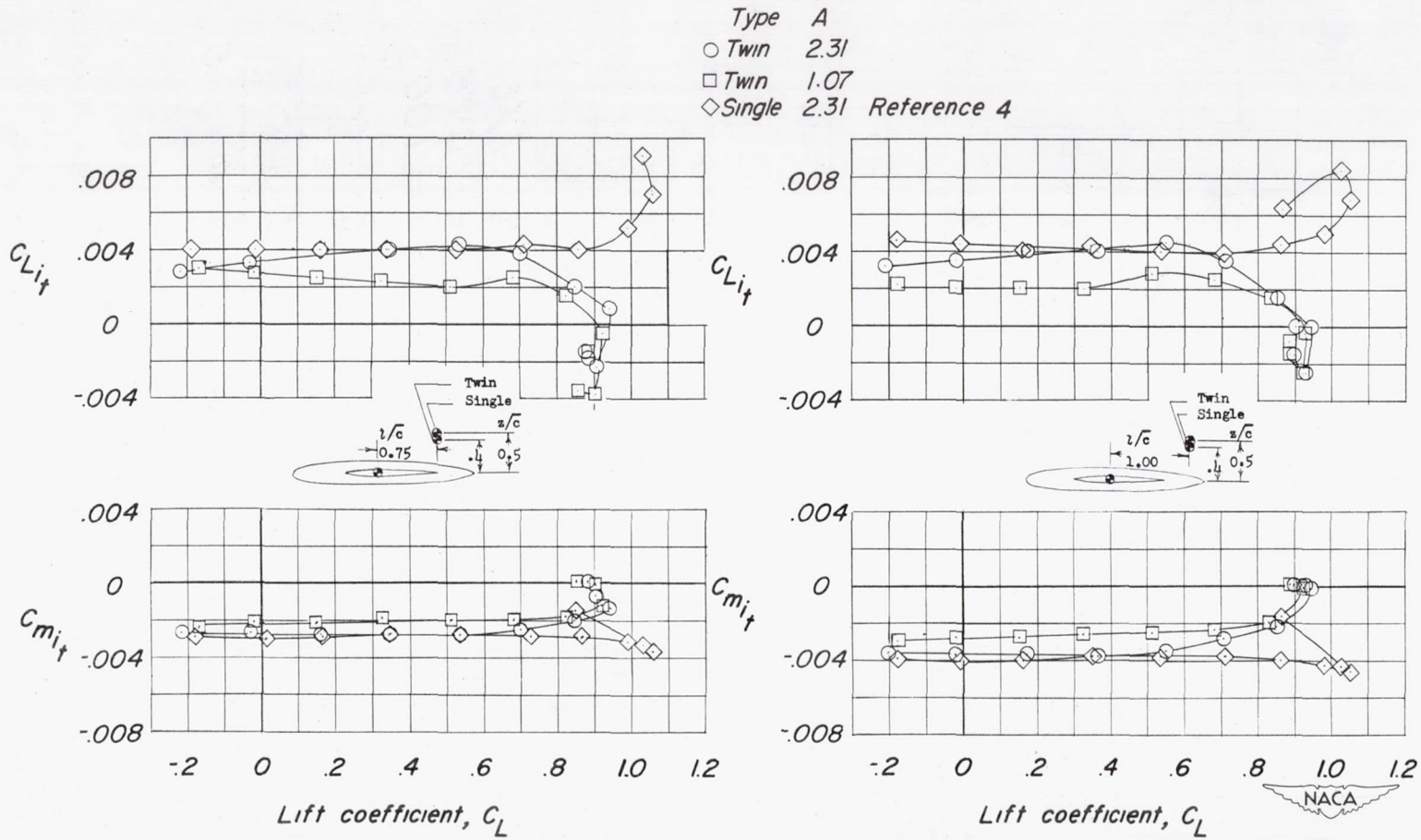

Figure 25.- Comparison of variation of $C_{L_{i_t}}$ and $C_{m_{i_t}}$ with C_L for a 60° triangular-wing model having twin or single triangular all-movable tails. Tail area, 10 percent of wing area. $C_{m_{C_L}} = -0.10$ at $C_L = 0$. (See text for centers of gravity.)

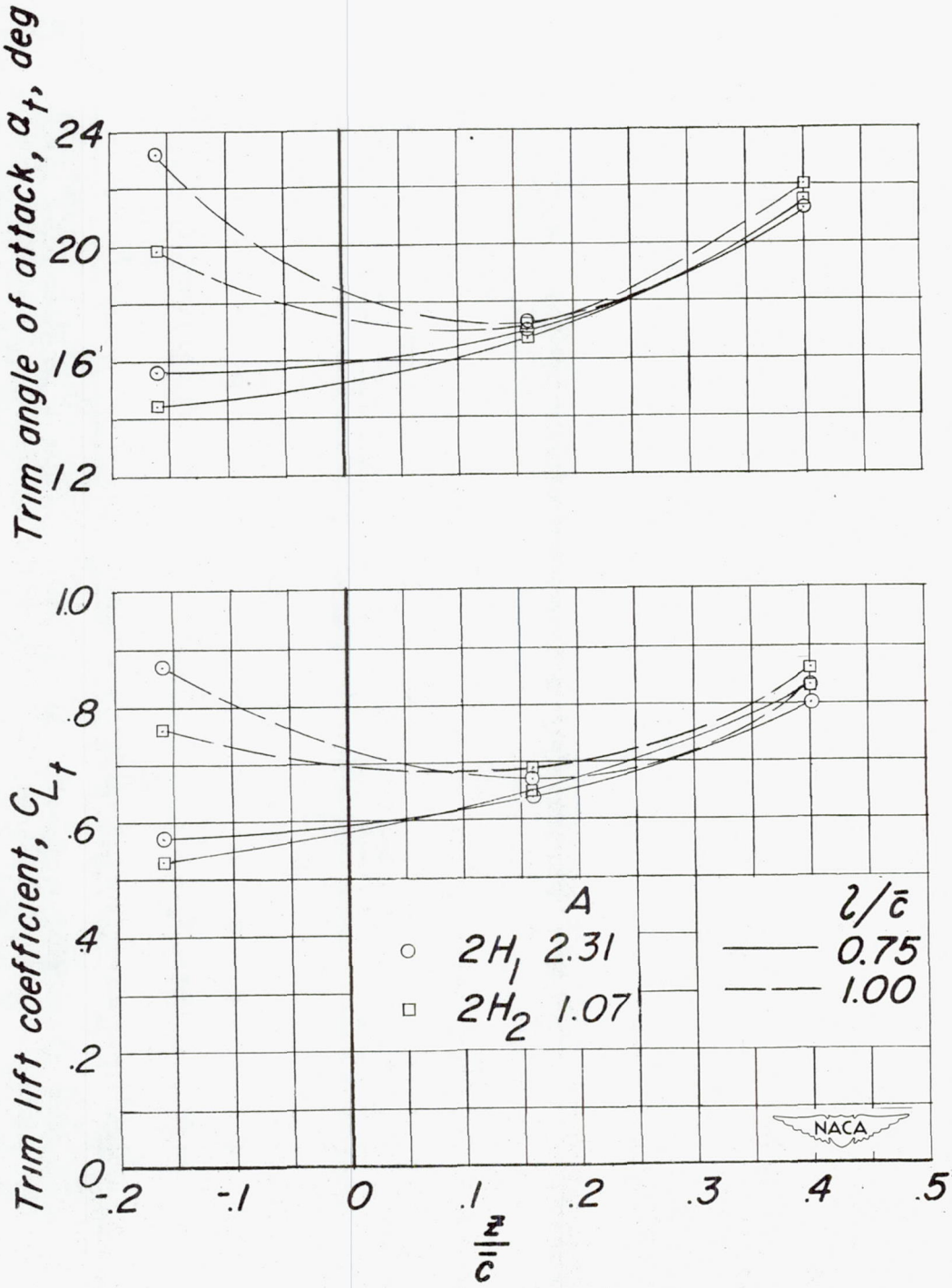

Figure 26.- Variation of trim lift coefficient and trim angle of attack with tail height for a 60° triangular-wing model having twin triangular all-movable tails. Tail area, 10 percent of wing area. $C_{m_{C_L}} = -0.10$ at $C_L = 0$. $i_t = -30°$.

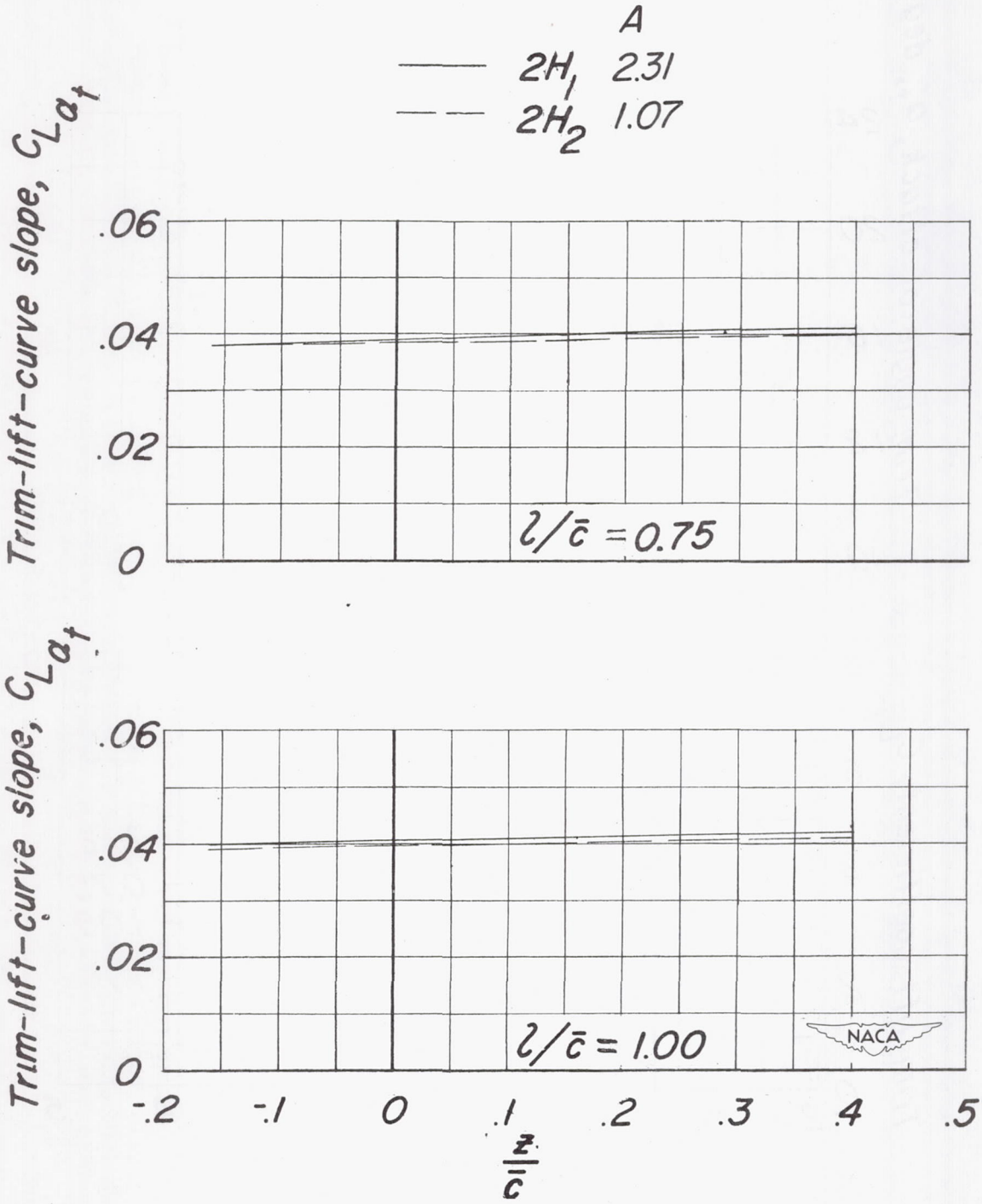

Figure 27.- Variation of trim-lift-curve slope with tail height for a 60° triangular-wing model having twin triangular all-movable tails. Tail area, 10 percent of wing area; $\alpha_t = 0^\circ$; $C_{m_{C_L}} = -0.10$.